ASSESSING THE CARBON EFFICIENCY OF BLUE-GREEN SPACES IN HIGH-DENSITY URBAN AREAS: A CASE STUDY OF XIAMEN ISLAND, CHINA

GUO, Q. M.[1] – WANG, Y. J.[2] – ZHANG, J. S.[3*] – XIE, H.[4] – QU, X. Y.[5]

[1]*Xi 'an University of Architecture and Technology, Xi'an 710311, China*
(e-mail: 18900221139@163.com)

[2]*Nanjing Forestry University, Nanjing 210037, China*
(e-mail: julia@njfu.edu.cn)

[3]*Department of Construction and Real Estate, School of Civil Engineering, Southeast University, Nanjing, China*
(e-mail: 230198129@seu.edu.cn)

[4]*School of Geography and Planning, Chizhou University, Chizhou, China*
(e-mail: xiehong@seu.edu.cn)

[5]*School of Engineering, The University of Manchester, Manchester, United Kingdom*
(e-mail: quxiuyu16@outlook.com)

[*]*Corresponding author*
e-mail: 230198129@seu.edu.cn

(Received 8th Sep 2025; accepted 3rd Dec 2025)

Abstract. Urban blue-green coupled spaces (UBGCS) are crucial for carbon sequestration and climate mitigation in dense cities. Yet, most studies examine blue and green spaces separately, limiting understanding of how their spatial coupling affects carbon sink efficiency. This study analyzed Xiamen Island, China, from 2000 to 2020 to quantify how coupled landscape patterns regulate net primary productivity (NPP). Carbon sequestration was estimated using the Carnegie Ames Stanford Approach (CASA), and spatial indicators characterized structural attributes and blue-green interactions. Results show three main findings. First, annual NPP exhibits a fluctuating upward trend with strong seasonality, with summer values substantially higher than winter values. Second, spatial coupling significantly enhances carbon sequestration: longer blue-green interfaces increase NPP, as indicated by the rise in the shape index of blue-green boundaries in Wuyuan Bay Wetland Park (SDGY) from 2.48 to 3.13, while reduced fragmentation improves ecological connectivity, shown by the decline in the fragmentation index (Ci) in Zhongshan Park (ZSGY) from 26.04 to 15.63. Third, seasonal drivers differ: boundary-length ratio dominates in summer, whereas green coverage rate is more influential in winter. These results provide actionable guidance for optimizing urban blue-green spatial design and improving carbon sink performance in dense cities.
Keywords: *urban blue–green space pattern, urban central area, net primary productivity, Carnegie-Ames-Stanford approach, spatial pattern*

Introduction

Increasing emissions of greenhouse gases have contributed significantly to global warming (Yuan et al., 2024; Dou et al., 2025; Zhang et al., 2025). In high-density urban areas, the fragmentation of urban green spaces and the increasing number of heat islands have further disrupted the carbon balance (Ng et al., 2011; Berardi, 2012; Martínez-Molina et al., 2016), highlighting the significant role of cities in carbon mitigation.

http://www.aloki.hu ● ISSN 1589 1623 (Print) ● ISSN 1785 0037 (Online)
DOI: http://dx.doi.org/10.15666/aeer/2401_959987

Urban Blue-Green Coupled Spaces (UBGCS) play a crucial role in balancing urban carbon cycles (Chen et al., 2024). Comprising natural, semi-natural, and artificial green and blue spaces (Foley and Kistemann, 2015; Yu et al., 2020), they are integral to urban ecosystems. These spaces provide multifunctional ecological benefits, including stormwater regulation (Su et al., 2018), microclimate moderation (Cheng et al., 2019), and enhanced carbon sequestration (He et al., 2020). The carbon sequestration (CS) pathways differ between green and blue spaces. Green spaces primarily sequester CO_2 through photosynthesis, with efficiency influenced by vegetation density (Mexia et al., 2018), species traits (Nowak et al., 2002), canopy structure (Yang et al., 2024), and soil properties (Kaye et al., 2005; Tang et al., 2019; Zhou et al., 2021; Yang et al., 2022, 2023). In contrast, blue spaces exhibit more complex carbon dynamics, with coastal wetlands and rivers acting as carbon reservoirs (Zhou et al., 2016; Duan and Huang, 2021; Wang et al., 2021). Urban blue spaces also contribute significantly to carbon sequestration via aquatic plant photosynthesis, soil carbon storage, and dissolved inorganic and organic carbon (McLeod et al., 2011; Short et al., 2016; Reiman and Xu, 2019).

The synergy between blue and green spaces enhances carbon sequestration beyond their individual contributions. Additionally, UBGCS help reduce emissions by mitigating heat islands, improving local climates, and promoting sustainable transportation (Zhang et al., 2022; Cheng et al., 2023). As such, UBGCS serve the dual purpose of enhancing carbon sinks and reducing emissions, making them key mechanisms for mitigating urban carbon footprints and rising CO_2 concentrations while alleviating ecological pressures (Chen et al., 2024). However, their fragmented distribution and scarcity in urban areas limit their full potential. In high-density cities, optimizing the spatial coupling of blue and green spaces is crucial for enhancing carbon sink efficiency and improving the ecological environment.

Previous studies on urban carbon sequestration (CS) have largely focused on green and blue spaces separately, with limited research on the relationship between the inner structure and layout of urban blue-green spaces (UGBS) and their CS potential. In urban green spaces, CS efficiency is influenced by factors such as vegetation density (Mexia et al., 2018), species traits (Nowak et al., 2002), canopy structure (Yang et al., 2024), and soil properties (Kaye et al., 2005; Tang et al., 2019; Zhou et al., 2021; Yang et al., 2022, 2023). In contrast, research on CS in blue spaces at the urban scale is sparse, with most studies concentrated on coastal wetlands, rivers, and lakes.

The exploration of carbon sequestration benefits within UGBS, based solely on individual green or blue space studies, is limited, highlighting the need for a more integrated approach. The synergistic mechanisms between blue and green spaces that promote CS are underexplored. Yuan et al. (2024) have pioneered research into the correlation between urban blue-green space patterns (UGBSP) and CS. Their XGBoost-SHAP model applied in Hefei quantified the influence of blue-green patterns on carbon sequestration, emphasizing the importance of patch complexity (LSI) and cohesion (Yuan et al., 2024); In Nanjing, their investigation using Landsat-8 and CASA models demonstrated the positive effects of landscape connectivity, showing that landscape percentage and aggregation index at the patch level enhanced CS, while negative correlations were found with zoning/shape index and non-significant results for maximum patch index (Yuan et al., 2023). While these studies consider UGBS as a whole and construct blue-green space pattern indicators, they do not examine the internal synergistic mechanisms governing the interactions between coupled elements,

http://www.aloki.hu ● ISSN 1589 1623 (Print) ● ISSN 1785 0037 (Online)
DOI: http://dx.doi.org/10.15666/aeer/2401_959987

limiting their ability to identify optimal spatial configurations for maximizing blue-green synergy.

This study aims to reveal the correlation between Urban Blue-Green Land (UBGL) spatial patterns and carbon sequestration benefits from a systemic perspective. Xiamen Island in Fujian Province, China, was chosen as the study area due to its unique natural environment and geographic constraints. As the political and economic core of Xiamen City, the island has limited land available for blue-green space development, making it crucial to explore strategies for enhancing carbon sink capacity within these restricted spaces. To address this gap, the study evaluates dynamic Urban Blue-Green Coupling Space Patterns (UBGCSP) in Xiamen's central urban area over two decades (2000–2020). Using multi-temporal remote sensing, meteorological data, and CASA-modeled NPP quantification, we construct UBGSP indicators to examine the relationships between spatial coupling attributes and fluctuations in carbon sequestration efficiency. The findings offer a paradigm shift, moving from scale-based expansion to efficiency-driven optimization of UBGCS, thereby advancing carbon-neutral planning for high-density cities.

Materials and methods

Study area

Xiamen City, a key sub-provincial city situated on China's southeastern coast, lies within the subtropical marine monsoon climate zone (*Fig. 1*), characterized by a moderate and wet climate. The vegetation on Xiamen Island is dominated by subtropical evergreen species. The primary tree species include Casuarina, camphor trees (such as camphor and large-leaf camphor), and banyan species (including small-leaf banyan and Indian banyan). Common shrubs include boxwood, holly, and rhododendron. These species form the core structure of urban green spaces across the island and represent the primary vegetation types influencing local ecological processes.

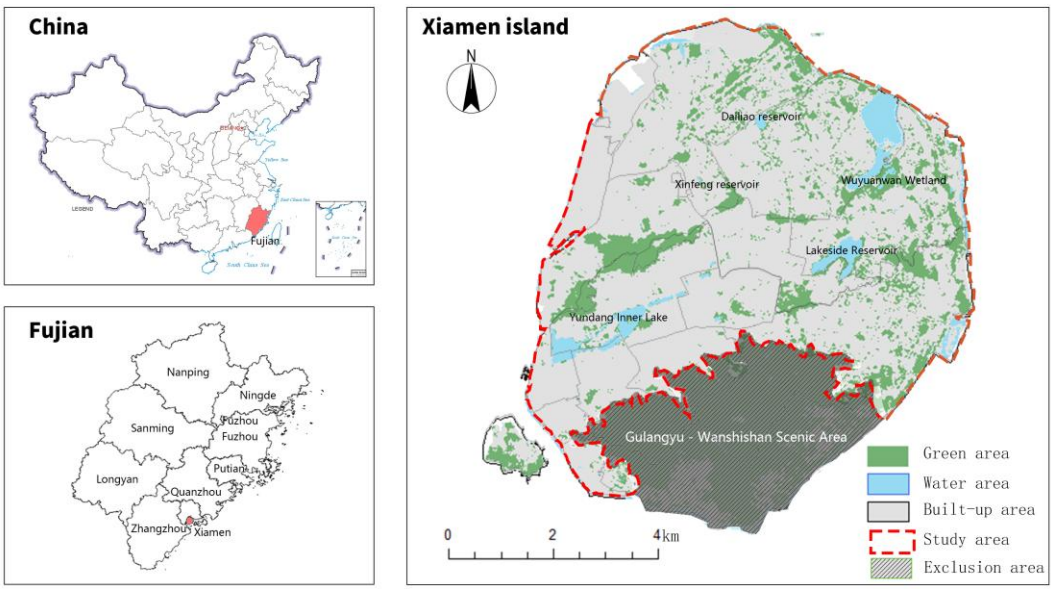

Figure 1. *Overview map of the study area on Xiamen Island, China*

http://www.aloki.hu ● ISSN 1589 1623 (Print) ● ISSN 1785 0037 (Online)
DOI: http://dx.doi.org/10.15666/aeer/2401_959987

As reported by the Xiamen Statistical Yearbook, the urbanization rate of the city rose significantly from 35% in 1980 to 90.19% by 2022. Over the same period, the urban land area expanded dramatically from 12 square kilometers in 1981 to 402 square kilometers in 2022, marking a nearly thirty-fold increase over four decades. However, the availability of space for further land development is now constrained. The research area of Xiamen Island, as delineated by documents such as the "Xiamen Municipal Overall Spatial Planning (2021-2035)" and the "Control Line Planning Map," consists of densely populated urban regions, notably Siming and Huli districts, which serve as the city's economic and political hubs. These districts span approximately 142 square kilometers, with a permanent resident population of 5.327 million, resulting in an urbanization rate of 100%, thus exemplifying a highly urbanized environment. The "Comprehensive Status Map of Green Spaces" identifies the Gulangyu-Wanshishan Scenic Area, which was excluded from the analysis to prevent the ecological effectiveness of large-scale scenic areas from influencing the outcome (Ren et al., 2013; Dong et al., 2024).

Xiamen Island, recognized as a national demonstration zone for ecological civilization, a national ecological garden city, and a sponge city with high aesthetic value, faces growing pressure to enhance its ecological environment. Rapid urbanization has led to high construction density and population concentration, severely limiting land available for blue-green coupling spaces. These spaces are often small, fragmented, and dispersed, hindering their ability to fully perform vital ecological functions such as climate regulation, air purification, and rainwater storage. Intensive human activity disrupts the ecological conditions of these spaces, while urban development and road networks further fragment the blue-green ecosystem. Many blue-green areas are designed primarily for aesthetic purposes, overlooking their essential ecological functions, including carbon sequestration. Ecological degradation in some regions has resulted in water pollution, vegetation loss, soil fertility decline, and reduced carbon sink capacity. Given the limited area of blue-green coupling spaces on Xiamen Island, improving their carbon sequestration efficiency is crucial.

Data collection and pre-processing

This study utilized land use, meteorological, vegetation type, NDVI, and NPP data (*Table 1*). The analysis was conducted across multiple time points to ensure accuracy and minimize potential errors from extreme weather events.

Land use data were sourced from the National Qinghai-Xizang Plateau Scientific Data Center (https://data.tpdc.ac.cn/home), with a spatial resolution of 30 m * 30 m. Remote-sensing images were processed using ENVI 5.2 software, including radiometric calibration, atmospheric geometric correction, and strip restoration. Using the China Land Use/Cover Classification (LUCC) system, the images were classified into six categories: cropland, forest, grassland, urban land, water bodies, and unused land. This classification provided land use data for Xiamen City in 2000, 2005, 2010, 2015, and 2020. Forests and grasslands were reclassified as green spaces, and water bodies as blue spaces, generating distribution maps for urban blue-green spaces in Xiamen Island across the five study years. These maps formed the basis for analyzing the spatial patterns of blue-green spaces.

Meteorological data, including monthly mean temperature, monthly total precipitation, and monthly solar radiation, were obtained from the National Qinghai-Xizang Plateau Scientific Data Center (https://data.tpdc.ac.cn/home) and EAR5_land

http://www.aloki.hu ● ISSN 1589 1623 (Print) ● ISSN 1785 0037 (Online)
DOI: http://dx.doi.org/10.15666/aeer/2401_959987

(https://cds.climate.copernicus.eu/#!/home). The meteorological dataset from the National Qinghai-Xizang Plateau Scientific Data Center was produced by Scholar Peng Shouzhang and has been independently validated using observations from 496 meteorological stations across China. Although the detailed locations of these stations are not publicly disclosed by the data provider, the validation results demonstrate high reliability, and the dataset has been widely used for regional environmental analyses. The data were clipped to the study area using ArcGIS 10.5 and converted into raster images with a spatial resolution of 30 m * 30 m for Xiamen Island. NDVI data were also acquired from the National Qinghai-Xizang Plateau Scientific Data Center, providing monthly NDVI data for all five study years with a 30 m * 30 m resolution.

Table 1. *Data sources and accuracy*

Data Type	Source	Resolution/ Accuracy	Time Range	Pre-treatment
Administrative boundary data	https://www.tianditu.gov.cn/		2020	After calibration with ArcGIS 10.5 projection, the vector was cropped to the range of Xiamen Island.
Land use data	https://data.tpdc.ac.cn/home	30m*30m	2020,2005,2010,2015,2020	Resampling to 30 meters using ArcGIS 10.5 → Projection matching →LUCC reclassification
Temperature data	https://data.tpdc.ac.cn/home	30m*30m	2020,2005,2010,2015,2020	Site data Kriging interpolation → 30-meter raster → monthly band synthesis
Precipitation data	https://data.tpdc.ac.cn/home	30m*30m	2020,2005,2010,2015,2020	The data was subjected to Kriging interpolation - resampled to a spatial resolution of 30 meters by 30 meters
Solar radiation data	https://cds.climate.copernicus.eu/#!/home)	30m*30m	2020,2005,2010,2015,2020	The data was subjected to Kriging interpolation - resampled to a spatial resolution of 30 meters by 30 meters
NDVI data	https://data.tpdc.ac.cn/home	30m*30m	2020,2005,2010,2015,2020	LUCC data mask clipping → Monthly time series synthesis.

Riverine green spaces are influenced by factors such as water flow and sediment deposition, while the spatial boundaries of coastal green spaces are challenging to define due to tidal fluctuations and seawater intrusion. In contrast, lake-green spaces (LG) typically have fixed spatial areas with clearly defined boundaries. When combined with surrounding green spaces, they form relatively closed carbon cycle units, creating more independent ecosystems that are easier to study. Therefore, this study investigates the carbon fixation efficiency of LG on Xiamen Island and performs a comparative analysis.

To minimize the interaction between the carbon sink effects of neighboring lake-green spaces and improve the reliability of the analysis, a 300-meter buffer zone was applied around each LG sample, following prior studies (Tan et al., 2021). This buffer eliminates potential spatial interference from adjacent LG patches, preserving data integrity in landscape pattern analysis.

Shoreline length and blue–green interface length were calculated directly from the reclassified thirty-meter raster layers. After reclassification, raster cells representing blue and green spaces were converted to vector polygons in ArcGIS 10.5. The shared boundaries between blue polygons and adjacent green polygons were extracted using the polygon adjacency tool. The total length of these shared boundaries, measured at the underlying spatial resolution of thirty meters, was defined as shoreline length for each

http://www.aloki.hu ● ISSN 1589 1623 (Print) ● ISSN 1785 0037 (Online)
DOI: http://dx.doi.org/10.15666/aeer/2401_959987

lake-green sample. This procedure ensured a consistent and reproducible measurement based on the same spatial resolution used for all other blue–green coupling indicators.

In line with these requirements, nine LG samples were selected (*Fig. 2*), ensuring no interference between them. The selected samples are: Zhongshan Park (ZSGY), Huli Park (cd2), Torch Park (cd3), Dialiao Reservoir Park (cd4), Hubian Reservoir Park (SK), Wuyuan Bay Wetland Park (SDGY), Yuandang Neihu area (cd6), Yuandang Hu area (cd7), and Bay Park (cd8).

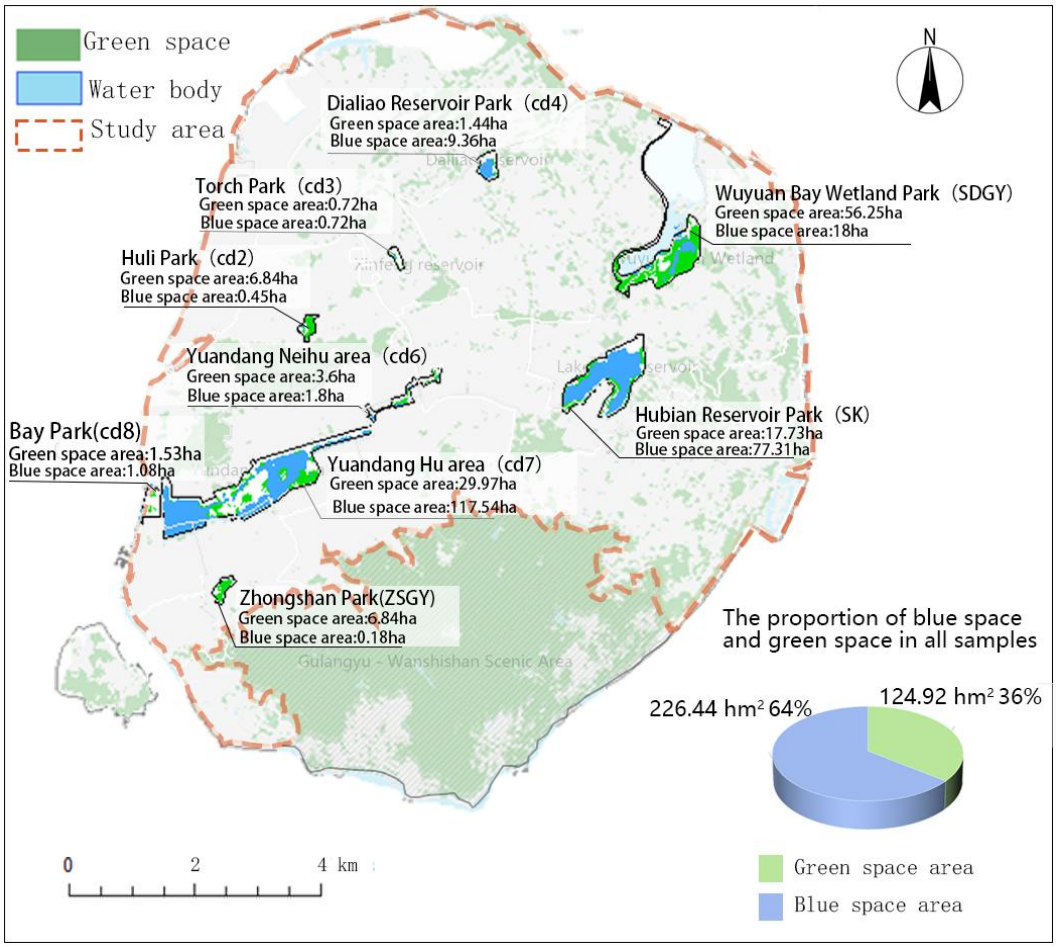

Figure 2. *Spatial distribution of sampled green and blue spaces on Xiamen Island, China*

Research framework

This study comprises four main components: data acquisition, data calculation, correlation analysis, and conclusion. The years 2000, 2005, 2010, 2015, and 2020 were selected as the research time points to minimize errors from remote sensing data precision and the impact of extreme weather conditions in any single year. First, landscape pattern indicators were chosen at two levels: the basic characteristics of blue-green spaces and the blue-green space coupling relationships, to quantify the spatial pattern of the UGBL. Next, the Carnegie-Ames-Stanford Biosphere (CASA) model was applied to calculate the NPP for the study area across the five years. Then, using SPSS 27, we established a relationship between the characteristics of the blue-green coupled space and the NPP model to evaluate how different spatial attributes influence carbon

http://www.aloki.hu ● ISSN 1589 1623 (Print) ● ISSN 1785 0037 (Online)
DOI: http://dx.doi.org/10.15666/aeer/2401_959987

sequestration. Finally, based on the correlation analysis results, we discuss potential strategies for optimizing the spatial layout of urban blue-green coupling spaces, as illustrated in the flowchart below (*Fig. 3*).

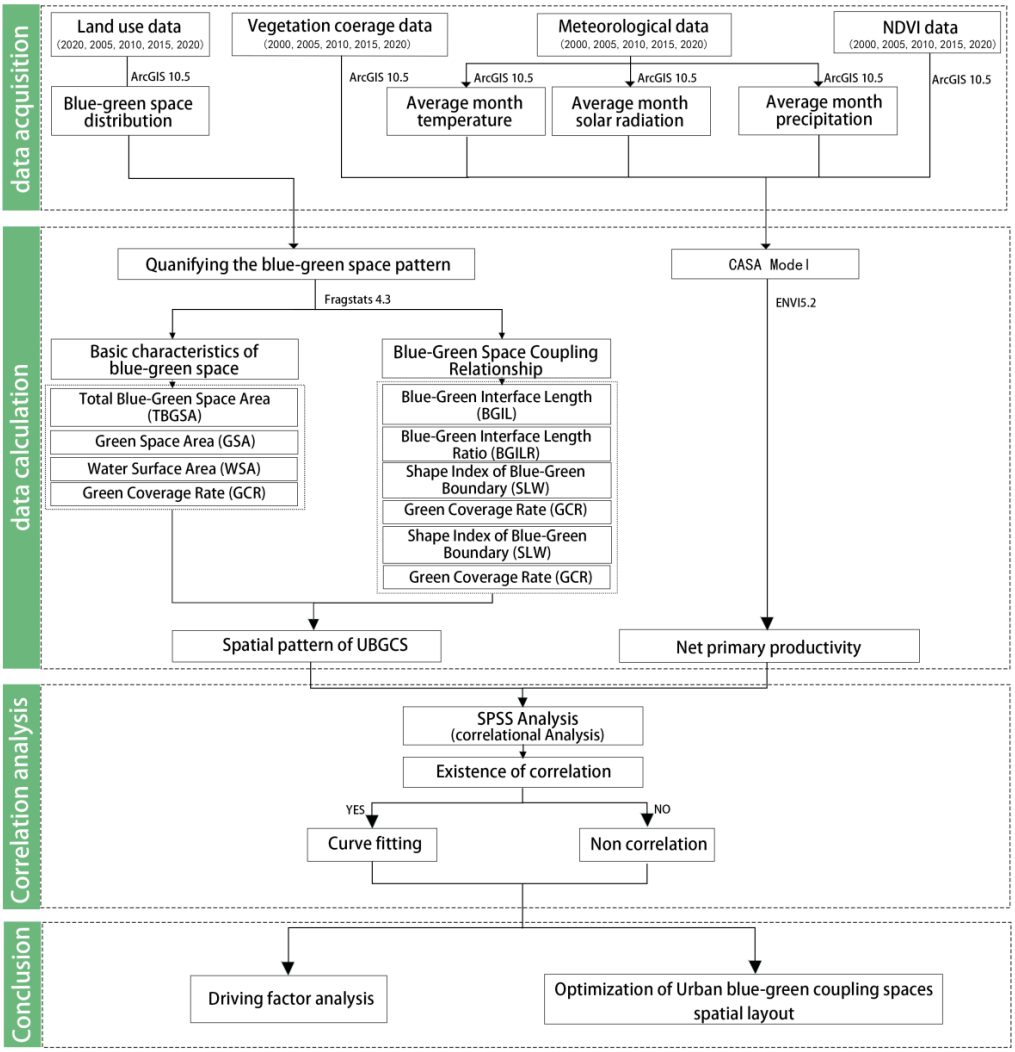

Figure 3. *Research flow of the study*

NPP calculation based on the CASA model

Net Primary Productivity (NPP) is the balance between carbon fixed by photosynthesis and carbon released through plant respiration. It represents the primary carbon input to ecosystems and serves as a key indicator of terrestrial ecosystem function, supporting material cycling and energy flow (Peng et al., 2016). Carbon sequestration occurs as ecosystems absorb and store atmospheric CO_2, with NPP providing a direct measure of sequestration intensity. NPP is therefore a key indicator of an ecosystem's carbon sink potential. This study applies the Carnegie–Ames–Stanford Approach (CASA) model, originally developed by Potter et al. (1993) which integrates remote sensing and meteorological data to simulate temporal dynamics of water, carbon, and nitrogen fluxes in terrestrial ecosystems. The CASA model is well suited for estimating NPP at regional scales, and its accuracy improves markedly when higher-

http://www.aloki.hu ● ISSN 1589 1623 (Print) ● ISSN 1785 0037 (Online)
DOI: http://dx.doi.org/10.15666/aeer/2401_959987

resolution remote sensing data are applied (Pan et al., 2011; Marshall et al., 2018). To calculate NPP, the CASA model relies on two key components: Absorbed Photosynthetically Active Radiation (APAR) and light use efficiency (ε), which are combined in the following equation:

$$NPP(x,t) = APAR(x,t) \times \varepsilon(x,t) \quad \text{(Eq.1)}$$

In *Eq. (1)*, NPP represents the net primary productivity of vegetation for pixel x in month t ($gC \cdot m^{-2} \cdot a^{-1}$), $APAR(x,t)$ denotes the absorbed photosynthetically active radiation by pixel x in month t ($gC \cdot m^{-2} \cdot month^{-1}$), and $\varepsilon(x,t)$ signifies the actual light use efficiency of pixel x in month t ($gC \cdot MJ^{-1}$).

The absorption of photosynthetically active radiation by vegetation depends on the solar radiation and plant characteristics. The expression for APAR is as follows:

$$APAR(x,t) = SOL(x,t) \times FPAR(x,t) \times 0.5 \quad \text{(Eq.2)}$$

In *Eq (2)*, $SOL(x,t)$ represents the total solar radiation received by pixel x in month t ($MJ \cdot m^{-2} \cdot month^{-1}$), $FPAR(x,t)$ signifies the fraction of incoming photosynthetically active radiation absorbed by the vegetation layer, and the constant 0.5 denotes the proportion of solar radiation utilized by vegetation out of the total solar radiation.

$$FPAR(x,t) = \alpha \times FPAR_{NDVI} + (1-\alpha) \times FPAR_{SR} \quad \text{(Eq.3)}$$

In *Eq (3)*, α represents the fraction of total solar radiation that vegetation can effectively harness. For the purposes of this study, we have chosen an adjustment coefficient of $\alpha = 0.5$.

$$\varepsilon(x,t) = T_{\varepsilon 1}(x,t) \times T_{\varepsilon 2}(x,t) \times W_{\varepsilon}(x,t) \times \varepsilon_{\max} \quad \text{(Eq.4)}$$

In *Eq (4)*, $T_{\varepsilon 1}(x,t)$ and $T_{\varepsilon 2}(x,t)$ represent the stress coefficients of light use efficiency due to monthly high and low temperatures, respectively; $W_{\varepsilon}(x,t)$ is the impact coefficient of water stress; $\varepsilon_{\max}$ stands for the maximum light use efficiency under ideal conditions ($gC \cdot MJ^{-1}$).

The NPP values for Xiamen Island's samples across five years were computed using the ENVI 5.3 platform and an NPP estimation module developed by Zhu et al. (2007).

Quantification of urban blue-green coupling spatial characteristics

Integrating water bodies and vegetated spaces in high-density urban areas through spatial adjacency and complementary ecological functions forms a coupled blue-green system that supports biodiversity and urban climate regulation. This network of water bodies and green spaces creates a composite structure through interfaces such as ecological revetments and greenways, enhancing ecological connectivity and fostering soil organic carbon deposition through water-land interactions, ultimately reducing CO_2. As a result, this integration produces a multi-layered effect that surpasses the individual functions of water systems or green spaces.

http://www.aloki.hu ● ISSN 1589 1623 (Print) ● ISSN 1785 0037 (Online)
DOI: http://dx.doi.org/10.15666/aeer/2401_959987

This coupled blue-green system serves as the basis for developing the blue-green space model and index system (Wang et al., 2023a). However, the lack of research on the coupling relationships of urban blue-green spaces at the site scale means there is no unified quantitative standard for evaluation. To assess the coupling degree between blue and green spaces, this study examines blue-green coupling differences across various spaces in the high-density areas of Xiamen City, constructing an index model that considers both the fundamental characteristics of blue-green spaces and their coupling relationships.

The basic characteristics of blue-green spaces focus on individual space attributes, while the coupling relationship metrics describe internal blue-green interactions within each study sample (*Table 2*). For basic characteristics, indicators include Total Blue-Green Space Area (TBGSA), Green Space Area (GSA), Water Space Area (WSA), and Green Coverage Rate (GCR), reflecting the area conditions of blue and green spaces.

Table 2. *Indicators of the spatial patterns of green-blue landscape*

Category	Name	Meaning	Calculation Formula	Reference
Basic Characteristics of Blue-Green Spaces	Total Blue-Green Space Area (TBGSA)	Total area of blue and green spaces (m^2)	/	Yu et al. (2021)
	Green Space Area (GSA)	Total green space area within the sample (m^2)	/	Huang et al. (2022)
	Water Surface Area (WSA)	Total water surface area within the sample (m^2)	/	Huang et al. (2022)
	Green Coverage Rate (GCR)	The ratio of the total green coverage area to the total selected area	$GCR = \frac{GSA}{Az}$ where GSA = green coverage area (m^2), Az = total selected area (m^2)	Huang et al. (2022)
Coupling Relationships of Blue-Green Spaces	Blue-Green Interface Length (BGIL)	Length of the interface between blue and green spaces	/	Huang et al. (2022)
	Blue-Green Interface Length Ratio (BGILR)	The ratio of BGIL to green space boundary length	$BGILR = \frac{BGIL}{GreenSpaceBoundaryLength}$	Huang et al. (2022)
	Shape Index of Blue-Green Boundary (SL_w)	The ratio of shoreline length to the perimeter of a circular water-body with the same area	$SL_W = \frac{L_W}{2 \times \sqrt{\pi \times Ag}}$ Where L_W = shoreline length (m), Ag = total water area (m^2)	Zhao et al. (2023)
	Blue-Green Area Ratio (BGAR)	The ratio of water surface area to green space area	$BGAR = \frac{WSA}{GSA}$ where WSA = water area (m^2), GSA = green area (m^2)	Wang et al. (2023b)
	Integration Degree (ID)	Transition between aquatic and terrestrial ecosystems within blue-green spaces	$ID = \frac{GSA}{TBGSA}$ where GSA = green coverage area (m^2), TBGSA = total blue-green area (m^2)	Wang et al. (2023b)
	Fragmentation Index (C_i)	Fragmentation of blue-green spaces within a unit area	$C_i = \frac{E}{WSA}$ where E = total boundary length of blue patches, WSA = total blue patch area (m^2)	Chen et al. (2016)

http://www.aloki.hu ● ISSN 1589 1623 (Print) ● ISSN 1785 0037 (Online)
DOI: http://dx.doi.org/10.15666/aeer/2401_959987

To quantify the coupling relationships and synergy, the metrics include Blue-Green Interface Boundary Length (BGIL), Blue-Green Boundary Length Ratio (BGILR), and Shape Index of Blue-Green Interface (SLW), which reflect edge complexity between blue and green spaces. Additionally, the Blue-Green Area Ratio (BGAR) and Integration Degree (ID) evaluate the configuration balance of blue and green spaces, while the Blue-Green Fragmentation Index (Ci) indicates fragmentation within the system. Utilizing spatial pattern analysis tools, this study quantifies the structural dynamics of blue-green coupled systems over five consecutive years, systematically evaluating their functional interdependencies.

Quantify the blue-green coupling spatial driving factors of carbon sequestration

Correlation analysis quantifies the direction and strength of relationships between variables using coefficients such as Pearson and Spearman. In this study it was applied to examine how spatial coupling metrics of blue-green areas relate to carbon sequestration efficiency. The analysis identifies the dominant spatial factors influencing sequestration, clarifies how the structural configuration of blue-green coupled spaces affects ecological functions, and provides empirical evidence to guide the optimization of urban blue-green infrastructure for advancing carbon neutrality.

Bivariate correlation analysis was used to quantify associations between blue-green spatial metrics and carbon sequestration efficiency (NPP). Key metrics such as area and boundary length were identified as potential drivers. Spearman's rank correlation coefficient was applied in SPSS 27.0 to examine synergistic (positive correlation) or inhibitory (negative correlation) effects of urban blue-green spatial patterns on carbon sequestration. A positive correlation is indicated by a coefficient $r > 0$, suggesting a synergistic relationship between the metric and CS, while $r<0$ denotes a negative correlation, implying an inhibitory effect on CS. The strength of the correlation was categorized as follows: strong correlation ($|r| \geq 0.5$), moderate correlation ($0.5 > |r| \geq 0.3$), weak correlation ($0.3>|r|\geq0.1$), and no correlation($|r| < 0.09$) (Cohen, 1977).

The influence of blue-green coupling indices on NPP was further examined through curve fitting (Li et al., 2011; Du et al., 2017), which identifies key drivers and quantifies each index's contribution to carbon sink efficiency, providing a basis for spatial optimization. Spearman correlation results served as the foundation for curve fitting. Characteristic indicators of Xiamen's blue-green coupling space were used as independent variables, with NPP as the dependent variable, and the best-fitting models were established in R Studio.

Results

The comparison of NPP among blue-green coupling spaces in Xiamen

The NPP calculation results are shown in figures (*Fig. 4*). A comparison of the five study years reveals significant temporal changes in carbon sink efficiency within Xiamen's high-density blue-green coupled spaces from 2000 to 2020. Overall, the NPP values for the samples exhibited a fluctuating upward trend. For instance, spring NPP in the ZSGY area increased from 34.66 $gC \cdot m^{-2} \cdot a^{-1}$ in 2000 to 38.69 $gC \cdot m^{-2} \cdot a^{-1}$ in 2020. Although summer NPP temporarily dropped to 27.38 $gC \cdot m^{-2} \cdot a^{-1}$ in 2010, it rebounded to 40.41 $gC \cdot m^{-2} \cdot a^{-1}$ by 2020. This recovery can likely be attributed to improvements in

http://www.aloki.hu ● ISSN 1589 1623 (Print) ● ISSN 1785 0037 (Online)
DOI: http://dx.doi.org/10.15666/aeer/2401_959987

blue-green coupling, ecological retrofitting, increased tree planting, and reduced impervious surface coverage, which enhanced vegetation density and soil carbon sequestration.

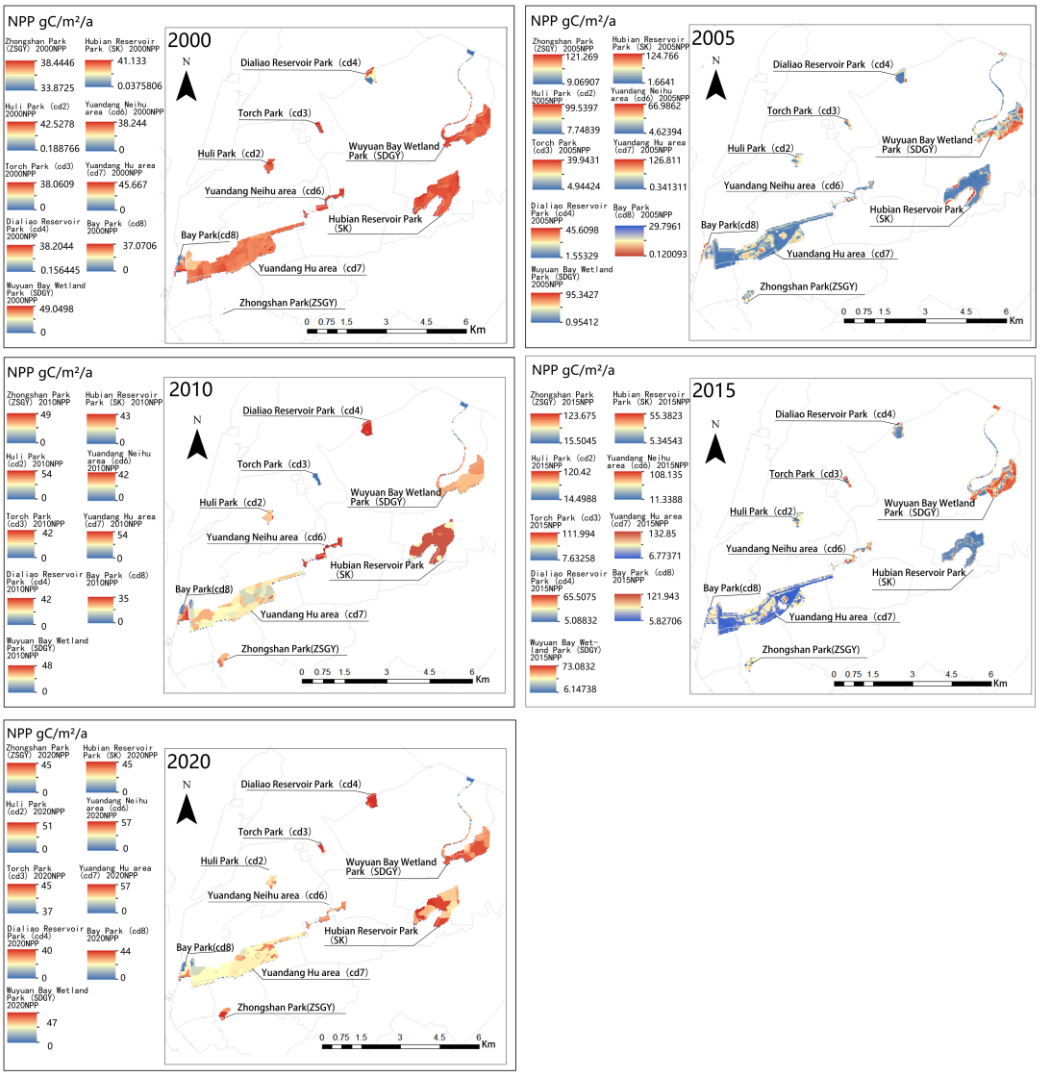

Figure 4. *The NPP calculation results of the blue and green space samples in the central urban area of Xiamen, China (2000–2020)*

Seasonal analysis showed that summer NPP consistently exceeded values from other seasons by 35 $gC \cdot m^{-2} \cdot a^{-1}$ to 62%, while winter NPP remained the lowest across all years. After 2015, seasonal fluctuations decreased, suggesting greater ecological stability in blue-green spaces. This pattern is likely explained by the warm, humid conditions in summer, which improve photosynthesis efficiency.

Spatial heterogeneity was observed as well. The cd8 area, which maintained stable dimensions from 2000 to 2020, consistently exhibited low NPP values. This is likely due to the overabundance of impervious surfaces and fragmented blue-green spatial patterns, disrupting carbon cycling and limiting microbial activity. In contrast, the SK area achieved a moderate NPP of 39.89 $gC \cdot m^{-2} \cdot a^{-1}$ in 2020 despite an imbalanced blue-

http://www.aloki.hu ● ISSN 1589 1623 (Print) ● ISSN 1785 0037 (Online)
DOI: http://dx.doi.org/10.15666/aeer/2401_959987

green area ratio (BGAR) of 0.81 $gC \cdot m^{-2} \cdot a^{-1}$. This suggests that optimized blue-green interface interactions can partially mitigate the effects of imbalanced area ratios.

Overall, the study demonstrates that the carbon sequestration capacity of blue-green infrastructure is influenced not only by the total area but also by the spatial configuration and functional integration of ecological components.

The spatial pattern of blue-green coupled space in Xiamen

The spatial patterns of the UBGCS indicators on Xiamen Island, as shown in *Fig. 5* and *Fig. 6*, reveal clear temporal changes in both the basic characteristics and the coupling relationships of blue–green spaces.

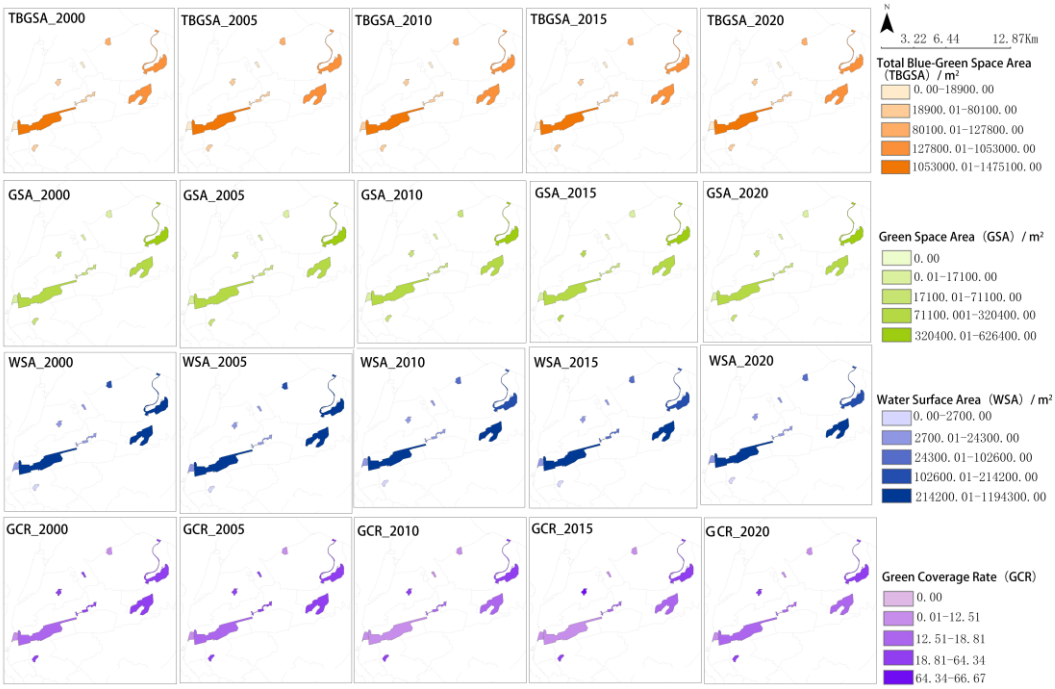

Figure 5. *Spatial patterns of basic landscape indicators describing blue–green coupled space on Xiamen Island, China (2000–2020)*

For the basic characteristics, the Green Space Area (GSA) and Green Coverage Rate (GCR) showed gradual increases across the five years, while the Water Surface Area (WSA) and Total Blue-Green Space Area (TBGSA) generally decreased annually.

Regarding the coupling relationships, the Integration Degree (ID) and Shape Index of Blue-Green Boundary (SLW) consistently increased, while the Blue-Green Interface Length Ratio (BGILR) and Blue-Green Interface Length (BGIL) fluctuated, indicating that the morphology of the blue-green boundary has become more complex over time.

The TBGSA varied across different areas. The ZSGY region remained stable, with a total area of 70,200 m^2 in both 2000 and 2020, while the cd2 area decreased from 80,100 m^2 to 72,900 m^2, reflecting a contraction of blue-green spaces in certain areas. The GSA exhibited an overall increasing trend. For example, the ZSGY area increased from 67,500 m^2 to 68,400 m^2, while the cd2 area grew from 71,100 m^2 to 68,400 m^2, indicating that the expansion of green spaces has been a primary focus. The WSA generally decreased, with the ZSGY area dropping from 2,700 m^2 to 1,800 m^2 and the

http://www.aloki.hu ● ISSN 1589 1623 (Print) ● ISSN 1785 0037 (Online)
DOI: http://dx.doi.org/10.15666/aeer/2401_959987

cd2 area decreasing from 9,000 m^2 to 4,500 m^2, suggesting a reduction in water space. The GCR fluctuated in sync with the GSA changes, such as in the SDGY area, where it rose from 44.80% in 2000 to 58.58% in 2020, confirming the increase in vegetation coverage (*Fig. 5*).

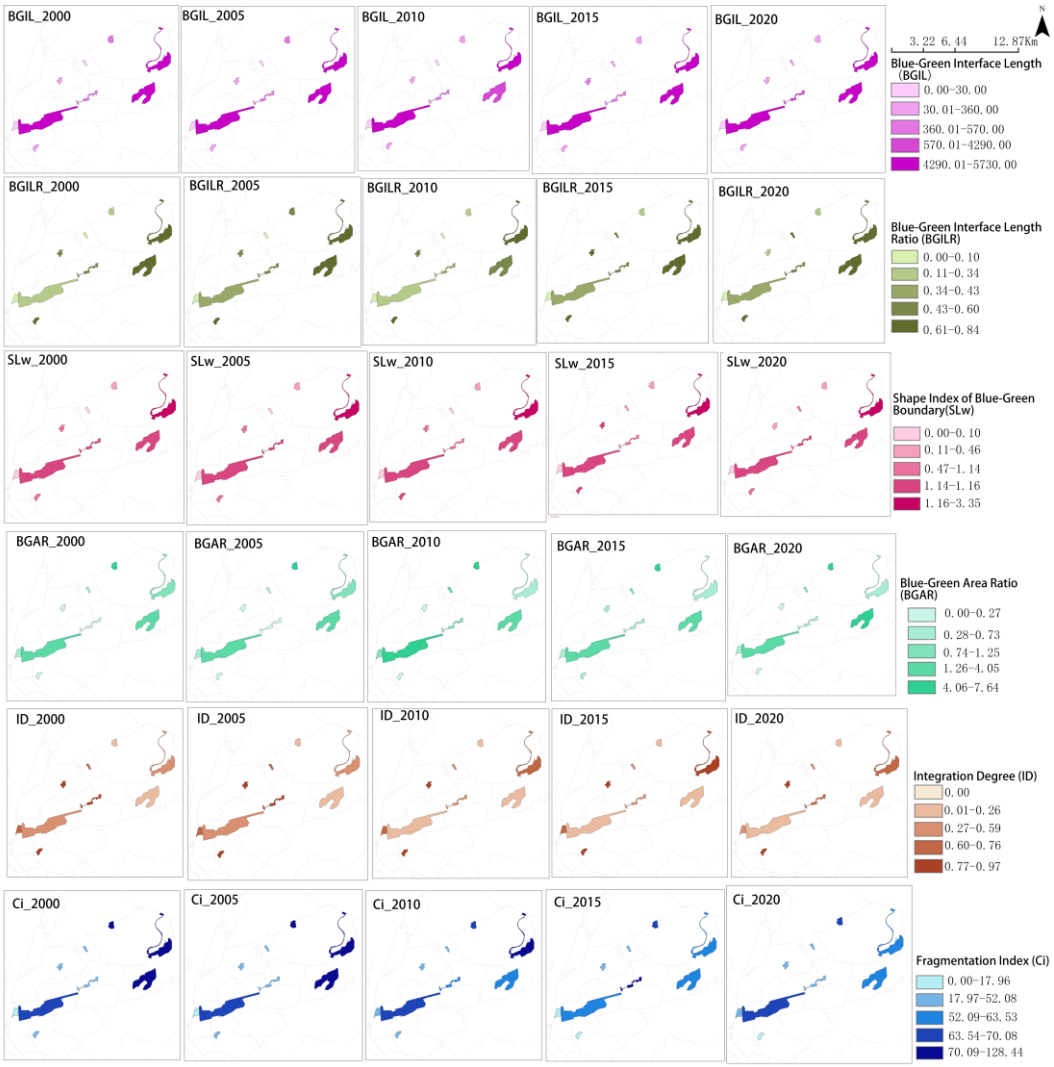

Figure 6. *Spatial patterns of blue–green coupling relationships on Xiamen Island, China (2000–2020)*

To supplement the spatial visualization in *Fig. 5*, all UBGCS indicators across all sites and years (12 indicators * 46 sites * 5 years) are compiled in *Table S1* (Supporting Information). Because this dataset is too large for the main text, a condensed summary of the key basic indicators (GSA, WSA, GCR, TBGSA) for all sites in 2000 and 2020 is provided in *Table 3*, enabling clear temporal comparison while maintaining readability.

For coupling relationship indicators, the BGIL and SLW varied by region. For example, in the SDGY area, SL_W increased from 2.4774 to 3.1317, indicating greater boundary complexity. The decrease in BGILR further supported the improvement in blue-green interaction efficiency. For example, in the ZSGY area, BGILR decreased from 0.7 to 0.667, and in the cd2 area, it dropped from 0.6 to 0.3.

http://www.aloki.hu ● ISSN 1589 1623 (Print) ● ISSN 1785 0037 (Online)
DOI: http://dx.doi.org/10.15666/aeer/2401_959987

Table 3. *Summary of key basic landscape indicators of blue–green coupled space on Xiamen Island (2000–2020)*

Site	Year	TBGSA (m^2)	GSA (m^2)	WSA (m^2)	GCR (%)
ZSGY	2000	70200	67500	2700	58.5938
ZSGY	2020	70200	68400	1800	59.375
cd2	2000	80100	71100	9000	60.3053
cd2	2020	72900	68400	4500	58.0153
cd3	2000	18900	11700	7200	18.8406
cd3	2020	14400	7200	7200	11.5942
cd4	2000	127800	17100	110700	10.7345
cd4	2020	108000	14400	93600	9.0395
SDGY	2000	855900	430200	425700	44.7985
SDGY	2020	742500	562500	180000	58.5754
SK	2000	1053000	236700	816300	19.8791
SK	2020	950400	177300	773100	14.8904
cd6	2000	54900	47700	7200	22.6496
cd6	2020	54900	36000	18000	17.094
cd7	2000	1450800	320400	1130400	13.6086
cd7	2020	1475100	299700	1175400	12.7294
cd8	2000	41400	11700.0000	29700	8.2803
cd8	2020	21600	15300.0000	10800	10.828

Note: GSA: Green Space Area; WSA: Water Surface Area; GCR: Green Coverage Rate; TBGSA: Total Blue-Green Space Area; BGAR: Blue-Green Area Ratio; ID: Integration Degree; Ci: Fragmentation Index. ZSGY: Zhongshan Park; cd2: Huli Park; cd3: Torch Park; cd4: Dialiao Reservoir Park; SK: Hubian Reservoir Park; SDGY: Wuyuan Bay Wetland Park; cd6:Yuandang Neihu area; cd7: Yuandang Hu area; cd8: Bay Park

Significant variations were observed in the Blue-Green Area Ratio (BGAR). For instance, the cd3 area saw an increase from 0.615 in 2000 to 1.0 in 2020, indicating an improved ratio of green space to water bodies. However, in the cd4 area, despite a high BGAR, NPP remained low, underscoring the negative impact of an imbalanced area ratio.

The general trend in most areas showed an improvement in the ID and a decrease in the Fragmentation Index (Ci). For example, in the ZSGY region, Ci decreased from 26.04 to 15.63, and in the cd2 area, it dropped from 50.89 to 25.45. In contrast, the cd8 region, with a high proportion of impervious surfaces and a BGILR of 0, exhibited consistently low NPP. The Ci in cd8 decreased from 74.31 to 25.48, highlighting the limitations of physical isolation on ecological functions (*Fig. 6*).

To support *Fig. 6*, a summarized comparison of key coupling indicators (BGIL, BGILR, SLW, BGAR, ID, Ci) for all sites in 2000 and 2020 is provided in *Table 4*. The complete dataset is available in *Table S1*.

Based on the calculated results of the spatial patterns of the UBGCS indicators in Xiamen Island, For the basic characteristics of blue-green spaces indicators, reflect the basic area conditions of the blue and green Spaces in the blue-green coupled space. The green Space Area (GSA), Green Coverage Rate (GCR) values gradually increased over the five study years. The Water Surface Area (WSA), Total Blue-Green Space Area (TBGSA), values decreased annually. Concerning the coupling relationships of blue-green spaces indicators, the proportion of integration degree (ID), shape index of blue-

http://www.aloki.hu ● ISSN 1589 1623 (Print) ● ISSN 1785 0037 (Online)
DOI: http://dx.doi.org/10.15666/aeer/2401_959987

green boundary (SLW) values showed a consistent annual increase, whereas the blue-green interface length ratio (BGILR) and blue-green interface length (BGIL) values fluctuate, this suggests that the morphology of the blue-green interaction boundary is becoming more complex.

Table 4. *Summary of key coupling relationship indicators of blue–green coupled space on Xiamen Island (2000–2020)*

Site	Year	BGIL	BGILR	SLW	BGAR	ID	Ci
ZSGY	2000	210	0.7000	1.1401	0.0400	0.9615	26.0417
ZSGY	2020	120	0.6667	0.7979	0.0263	0.9744	15.625
cd2	2000	360	0.6	1.0705	0.1266	0.8876	50.8906
cd2	2020	90	0.3	0.3785	0.0658	0.9383	25.4453
cd3	2000	30	0.1	0.0997	0.6154	0.619	48.3092
cd3	2020	150	0.625	0.4987	1	0.5	38.6473
cd4	2000	540	0.439	0.4578	6.4737	0.1338	77.2128
cd4	2020	360	0.3243	0.3319	6.5	0.1333	69.6798
SDGY	2000	5730	0.8197	2.4774	0.9895	0.5026	74.31
SDGY	2020	4710	0.801	3.1317	0.32	0.7576	61.2309
SK	2000	5250	0.7813	1.6392	3.4487	0.2248	72.7898
SK	2020	4500	0.6522	1.4437	4.3604	0.1866	57.9491
cd6	2000	420	0.5385	1.3963	0.1509	0.8689	37.037
cd6	2020	600	0.5882	1.2616	0.5	0.6667	48.433
cd7	2000	5400	0.3557	1.4328	3.5281	0.2834	64.475
cd7	2020	5670	0.375	1.4753	3.9219	0.255	64.2202
cd8	2000	30	0.0286	0.0491	2.5385	0.2826	74.31
cd8	2020	0	0.0000	0	0.7059	0.5862	25.4777

Note: GIL: Blue–Green Interface Length; BGILR: Blue–Green Interface Length Ratio; SLW: Shape Index of Blue–Green Boundary; BGAR: Blue–Green Area Ratio; ID: Integration Degree; Ci: Fragmentation Index. ZSGY: Zhongshan Park; cd2: Huli Park; cd3: Torch Park; cd4: Dialiao Reservoir Park; SK: Hubian Reservoir Park; SDGY: Wuyuan Bay Wetland Park; cd6:Yuandang Neihu area; cd7: Yuandang Hu area; cd8: Bay Park

The relationship of various UBGCS indicators with NPP

The results from the Spielman correlation analysis presented in figures (*Fig. 5*) reveal notable spatio-temporal variation in the relationship between the blue-green coupling spatial index and overall as well as seasonal carbon sink efficiency (NPP). The Blue-Green Area Ratio (BGAR) was significantly negatively correlated with overall carbon sink efficiency ($r = -0.367$, $p = 0.013$), suggesting that a high proportion of water body area can reduce carbon sink capacity. Conversely, the Blue-Green Integration Degree (ID) showed a significant positive correlation with overall NPP ($r = 0.363$, $p = 0.014$). For instance, in the ZSGY region, winter NPP increased by 106.5% (from 16.04 to 33.13) as the ID rose from 0.961 to 0.974, demonstrating the positive impact of spatial interweaving on carbon sink efficiency. Additionally, a weak negative correlation between the Water Surface Area (WSA) and overall NPP ($r = -0.307$, $p = 0.041$) indicates that limiting the expansion of water bodies is crucial to preserving green space and maintaining carbon sequestration.

In terms of seasonal analysis, spring carbon sink efficiency was potentially influenced by the Green Coverage Rate (GCR) ($r = 0.292$, $p = 0.051$). In the SDGY

http://www.aloki.hu ● ISSN 1589 1623 (Print) ● ISSN 1785 0037 (Online)
DOI: http://dx.doi.org/10.15666/aeer/2401_959987

area, as the GCR increased from 44.80% to 58.58%, spring NPP stabilized at 38.25, highlighting the key role of vegetation coverage in enhancing photosynthesis. The weak positive correlation of the ID in spring ($r = 0.242$, $p = 0.109$) suggests that optimizing vegetation types in combination with spatial integration is necessary. For instance, in the d3 area, targeted tree planting maintained spring NPP (38.30), despite a decrease in integration levels (from 0.62 to 0.5), demonstrating that functional complementarity can stabilize ecological outcomes.

In summer, carbon sink efficiency was influenced by both the Blue-Green Boundary Length Ratio (BGILR) ($r = 0.256$, $p = 0.090$) and GCR ($r = 0.396$, $p = 0.007$). In the cd2 area, an increase in BGILR from 0.6 to 0.65 led to a significant rise in summer NPP from 44.73 to 112.80. Similarly, in the SK region, optimizing GCR helped stabilize summer NPP at 55.79, emphasizing the synergistic effects of boundary interaction efficiency and vegetation density in high-temperature environments.

In autumn, the BGAR showed a significant negative correlation with carbon sink efficiency ($r = -0.335$, $p = 0.024$). In the cd4 region, a persistently high BGAR of 6.47 resulted in a low autumn NPP of 54.90. However, in the ZSGY region, autumn NPP increased from 27.38 to 40.41 by improving the ID (from 0.961 to 0.974), demonstrating that spatial interweaving can partially mitigate the limitations imposed by the area ratio.

In winter, NPP was inhibited by blue-green fragmentation (Ci) ($r = -0.162$, $p = 0.289$). In the cd6 region, when Ci surged to 128.44 in 2015, winter NPP dropped sharply to 11.37. However, after Ci decreased to 48.43 in 2020, winter NPP rebounded to 26.57, indicating that fragmentation disrupts the carbon cycle in low-temperature environments. Additionally, a weak positive correlation between the ID and winter NPP ($r = 0.212$, $p = 0.162$) led to a significant increase in winter NPP in the ZSGY region, highlighting the buffering potential of spatial interaction to mitigate low-temperature stress.

Curve fitting was applied to nine spatial characteristic indicators of blue-green coupling in Xiamen. Among these, GSA showed significant seasonal fluctuations and variation in vegetation types affecting NPP. The peak NPP value of approximately 50 $gC \cdot m^{-2}$ (*Fig. 7b*, $R^2 = 0.05$) occurred in the high-value range of WSA during summer. However, efficacy decreased notably in autumn and winter due to eutrophication and low temperatures (*Fig. 7b*, $R^2 = 0.05$-0.01). The average NPP of GCR was relatively high within the 40%-60% coverage range in autumn (*Fig. 7c*, $R^2 = 0.16$). BGIL exhibited a weak positive correlation in both summer and autumn (*Fig. 7e*, $R^2 = 0.14$-0.15). In spring, NPP increased as BGILR rose (*Fig. 7f*, $R^2 = 0.09$). For some samples, NPP reached 40-50 $gC \cdot m^{-2}$ within the BGILR range of 0.4-0.6, with the correlation strengthening in summer (*Fig. 7f*, $R^2 = 0.14$). For high BGILR samples, NPP partially increased to 60 $gC \cdot m^{-2}$, likely due to higher temperatures promoting water-land material exchange and enhancing photosynthesis of submerged plants. The correlation between BGILR and NPP was strongest in autumn (*Fig. 7f*, $R^2 = 0.15$), suggesting that moderate blue-green spatial interface interactions can improve carbon sink efficiency.

In summer, some samples with high SLW values showed a slight increase in NPP, reaching a peak of approximately 40 $gC \cdot m^{-2}$. This is likely due to the complex shoreline, which facilitates water-land interactions and enhances carbon sink efficiency. The influence of BGAR on NPP exhibited significant seasonal variability and a nonlinear threshold effect. In spring, the BGAR fitting curve showed a weak positive

http://www.aloki.hu ● ISSN 1589 1623 (Print) ● ISSN 1785 0037 (Online)
DOI: http://dx.doi.org/10.15666/aeer/2401_959987

correlation (*Fig. 8h*, $R^2 = 0.09$), suggesting that a balanced blue-green ratio can improve carbon sink efficiency. The correlation was stronger in summer (*Fig. 8h*, $R^2 = 0.14$), potentially due to the evaporative cooling of water bodies that promotes vegetation photosynthesis during high summer temperatures. The performance of ID and Ci was constrained by an excessive proportion of hard substrates or fragmentation in carbon cycle channels ($R^2 = 0.12$ in spring). The results of the fitting curve analysis are presented in figures (*Fig. 9*).

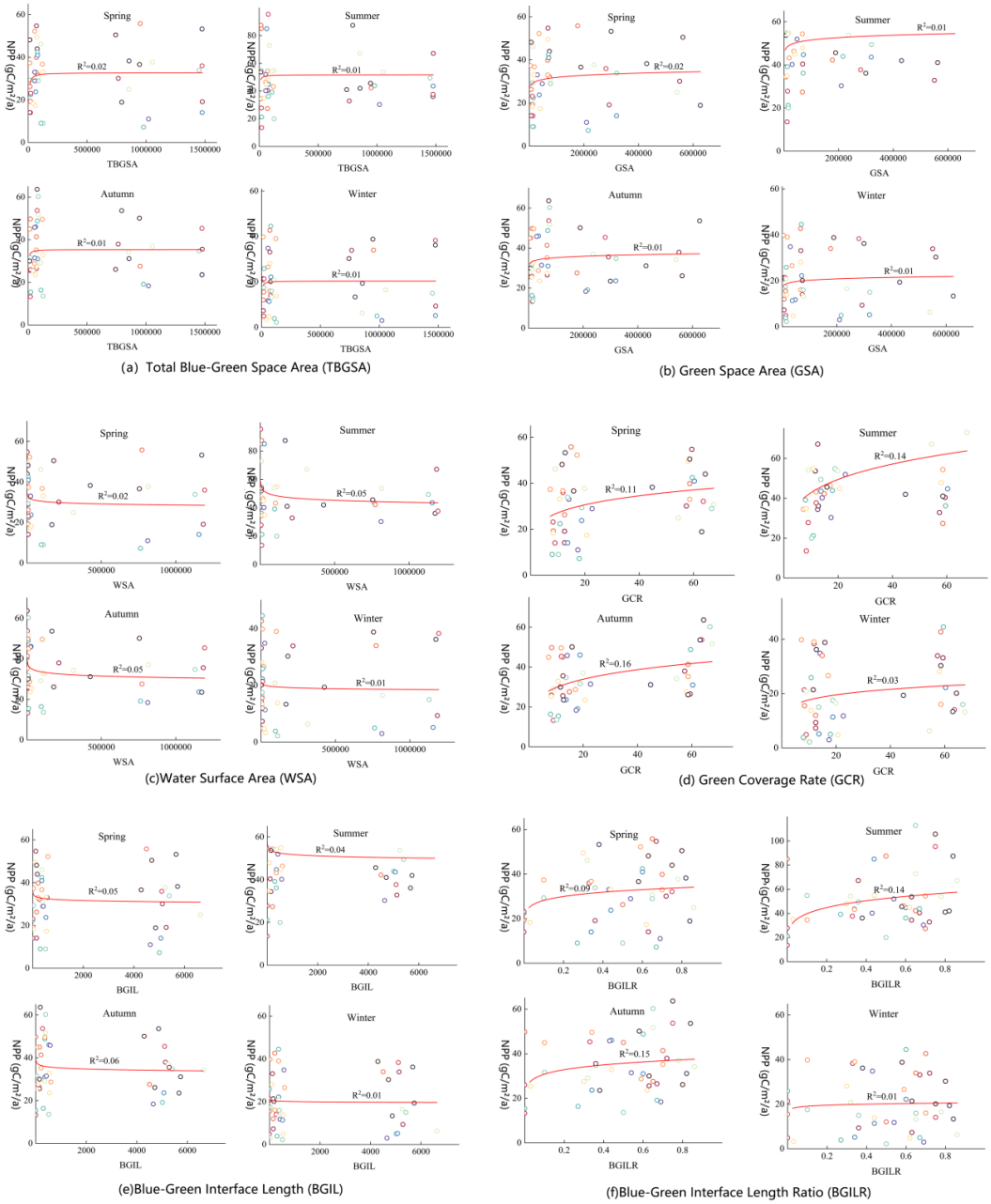

Figure 7. *Curve fitting between Net Primary Productivity and (a) Total Blue-Green Space Area (TBGSA), (b) Green Space Area (GSA), (c) Water Surface Area (WSA), (d) Green Coverage Rate (GCR), (e) Blue-Green Interface Length (BGIL), (f) Blue-Green Interface Length Ratio (BGILR) on Xiamen Island, China, from 2000 to 2020*

http://www.aloki.hu ● ISSN 1589 1623 (Print) ● ISSN 1785 0037 (Online)
DOI: http://dx.doi.org/10.15666/aeer/2401_959987

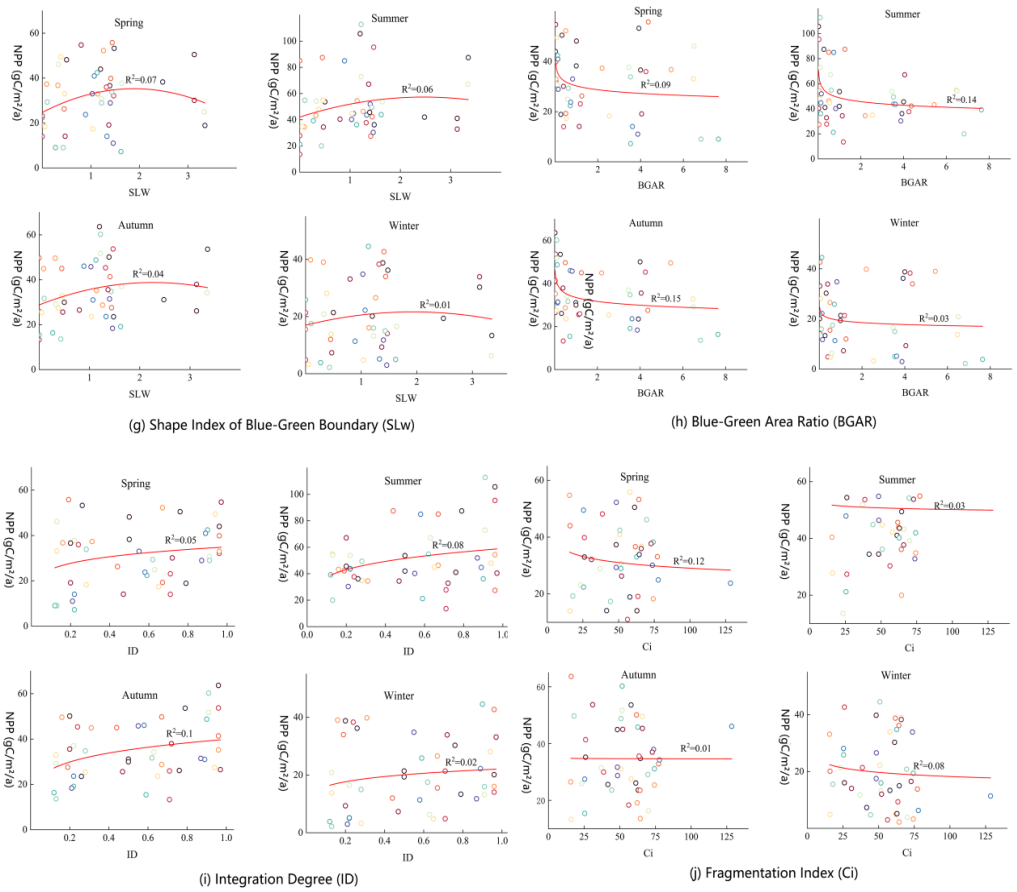

Figure 8. *Curve fitting between Net Primary Productivity and (g) Shape Index of Blue-Green Boundary (SLw), (h) Blue-Green Area Ratio (BGAR), (i) Integration Degree (ID), (j) Fragmentation Index (Ci) on Xiamen Island, China, from 2000 to 2020*

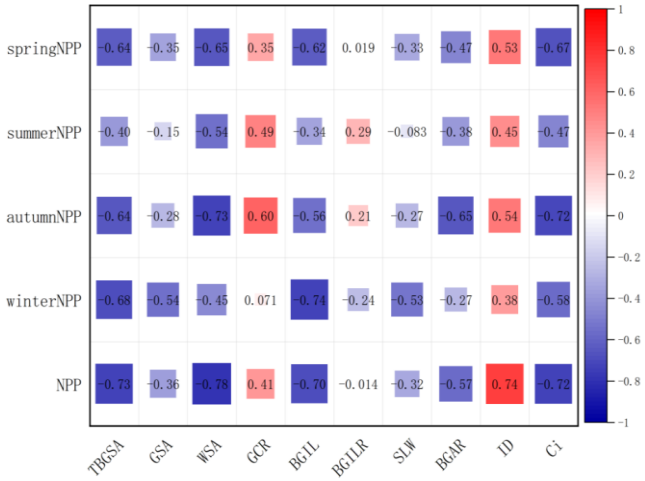

Figure 9. *Correlation analysis of seasonal blue-green coupling indicators and carbon sequestration factors on Xiamen Island, China, from 2000 to 2020. Note: TBGSA: Total Blue-Green Space Area; GSA: Green Space Area; WSA: Water Surface Area; GCR : Green Coverage Rate; BGIL : Blue-Green Interface Length; BGILR : Blue-Green Interface Length Ratio; SLW : Shape Index of the Blue-Green Interface; BGAR : Blue-Green Area Ratio; ID : Integration Degree; Ci :Blue-Green Fragmentation Index*

http://www.aloki.hu ● ISSN 1589 1623 (Print) ● ISSN 1785 0037 (Online)
DOI: http://dx.doi.org/10.15666/aeer/2401_959987

Discussion

Influence of urban blue-green coupled spaces spatial pattern on CS

The carbon sink efficiency of blue-green coupled spaces in the high-density area of Xiamen is influenced by the strength of the coupling between their spatial configuration and ecological processes. A quantitative analysis of the carbon sink efficiency in these spaces from 2000 to 2020 was conducted using the CASA model. Longitudinal analysis reveals that, despite urban densification limiting the area of blue-green space, annual carbon sequestration rates increased by 1.3% with a reduction in seasonal variability. These trends suggest that ecological resilience is closely linked to spatial expansion, optimized landscape configuration, and functional complementarity. However, the characteristics of high-density urban areas enhance the carbon sink efficiency of blue-green coupled spaces, with the efficiency being more dependent on spatial optimization than on area expansion. For example, smaller samples achieved an average annual NPP growth rate of 1.9% by optimizing vegetation types, such as replacing lawns with trees, which significantly outperformed larger samples. This confirms the need for intensive configuration in high-density areas. Although samples dominated by impervious surfaces have a larger area than some others, their lower degree of blue-green coupling, combined with the negative effects of hard surfaces and human interference, results in the highest fragmentation among all samples. This fragmentation disrupts ecological connectivity and hinders material circulation. Hard revetments and pavements absorb heat, exacerbating the local heat island effect. The surface temperature is higher than that of natural revetment areas, directly reducing the photosynthetic efficiency of vegetation. The spatial configuration of aquatic and vegetated areas in this region shows limited connectivity, diminishing their capacity for integrated hydrological and ecological functions. The introduction of green corridors could enhance these interactions, promoting climate adaptation and supporting biodiversity.

In contrast, the length ratio of the SDGY blue-green boundary increased to 0.45, resulting in greater complexity in the interaction interface between water bodies and vegetation. Consequently, the NPP value increased from 32.45 $gC \cdot m^{-2}$ in 2010 to 36.72 $gC \cdot m^{-2}$ in 2020. This comparison highlights that the difference in carbon sink efficiency between blue and green spaces is not solely dependent on area size; instead, it reflects the quality of spatial coupling. Further analysis reveals that highly efficient blue-green coupling areas generally exhibit the following characteristics. First, the integration of water bodies and green spaces within a networked structure. For example, some areas are connected to green spaces via a lake-ring greenway, forming a composite structure of blue veins and green veins, which facilitates material exchange between carbon sink patches. Second, the ecological design of boundary forms, such as stepped vegetation slope protection and stone revetments, which can reduce soil erosion and increase the soil's organic matter content through root carbon sequestration. It indicates that the increase of carbon sinks in high-density areas needs to break away from the traditional thinking of area first and turn to the refined path of optimizing spatial forms and strengthening ecological processes. The analysis reveals that spatial configuration within blue-green infrastructure systems, such as shape complexity and connectivity, exerts a stronger influence on carbon sequestration efficiency than total area, emphasizing that functional optimization, rather than mere spatial expansion, is critical.

http://www.aloki.hu ● ISSN 1589 1623 (Print) ● ISSN 1785 0037 (Online)
DOI: http://dx.doi.org/10.15666/aeer/2401_959987

Influencing factors of carbon sink efficiency in different seasons

The carbon sink efficiency in blue-green coupled spaces exhibits significant seasonal variation. The average NPP in summer (45.32 $gC \cdot m^{-2}$) is 2.34 times higher than in winter (19.38 $gC \cdot m^{-2}$). This difference is closely tied to the climatic characteristics of Xiamen, with summer temperatures averaging 28℃ and high humidity, and winter temperatures averaging 13℃ with dry conditions. The high summer temperatures and humidity promote photosynthesis, significantly boosting the carbon assimilation rate in both aquatic plants and trees. For example, in the ZSGY area, the peak NPP in summer reaches 55.76 $gC \cdot m^{-2}$. The strategic design of natural banks and multi-layered vegetation along water bodies enhances water evaporation and plant transpiration, contributing to a ‘cold island effect’ that lowers surface temperatures and alleviates thermal stress in urban areas.

In contrast, the low temperatures and dry conditions in winter limit vegetation activity, particularly reducing the photosynthetic rate of evergreen trees, leading to a significant decline in carbon sink efficiency. This seasonal pattern reflects the phenological characteristics of vegetation in subtropical monsoon climates. The primary driving factors also differ by season. In summer, the length of the blue-green boundary is the key positive indicator of carbon sink efficiency. This supports the "edge effect" theory: a longer water-land interface enhances material exchange, facilitating organic carbon storage in sediments through increased oxygen flow, nutrient circulation, and microbial activity. The extended water-land interaction interface also creates diverse marginal habitats, supporting submerged, floating-leaf, and emergent plants that further enhance carbon absorption.

In winter, carbon sink efficiency is mainly influenced by green coverage. The canopy density of cold-tolerant vegetation reduces surface heat loss and helps maintain root system activity. These results underscore the multifunctionality of blue-green spaces and highlight how seasonal changes require different design strategies. In summer, emphasis should be placed on optimizing water body boundary morphology. Transforming natural revetments and extending the blue-green interaction interface, along with stepped planting of submerged and emergent plants, can improve carbon sink efficiency per unit area. In winter, focus should be on selecting appropriate vegetation types and creating microclimates. For example, planting cold-resistant shrubs around hard surfaces and using permeable materials can reduce carbon loss from surface runoff.

Additionally, cross-seasonal strategies are essential. Preserving the litter cover layer can suppress CO_2 from soil respiration in winter, while in summer, the layer can decompose into humus, enhancing carbon sequestration. This dynamic, adaptive design not only highlights the multifunctionality of blue and green spaces but also offers a flexible approach for high-density cities to mitigate climate change impacts.

Comparison with existing literature

Our findings align with and extend previous studies on urban spatial configuration and carbon sequestration. Prior research in Nanjing (Yuan et al., 2023, 2024). identified landscape cohesion indicators—such as PLAND and AI—as positive drivers of NPP, whereas shape and fragmentation metrics (LSI, DIVISION) had negative effects. This parallels our finding that increased green coverage and reduced fragmentation enhance

http://www.aloki.hu ● ISSN 1589 1623 (Print) ● ISSN 1785 0037 (Online)
DOI: http://dx.doi.org/10.15666/aeer/2401_959987

carbon uptake, confirming that spatial cohesion is a universal driver across urban contexts.

However, our study advances beyond traditional patch-based analysis by explicitly quantifying blue–green coupling, using metrics such as Blue–Green Interface Length Ratio (BGILR), Integration Degree (ID), and Fragmentation Index (Ci). Previous models identified ED and COHESION as influential factors but did not capture joint water–land processes. Our results demonstrate that functional coupling, rather than isolated blue or green patches, is critical for maximizing carbon performance—particularly in dense cities where land scarcity necessitates efficient spatial synergies.

Moreover, our seasonal differentiation contributes novel insights. While earlier studies used static annual averages, our analysis shows that summer carbon uptake is predominantly driven by boundary morphology (BGILR), whereas winter performance depends more strongly on vegetation structure (GCR). This temporal perspective highlights the need for adaptive, climate-responsive spatial design—an aspect largely absent from the existing literature.

Overall, by integrating coupling-specific metrics and seasonal dynamics, this study fills a key gap in understanding how blue–green interactions shape urban carbon sequestration, offering a more comprehensive interpretation than previous landscape-pattern studies.

Suggestions for optimizing blue-green coupling space based on the improvement of CS

Achieving carbon neutrality and carbon peaking is a critical strategy to combat global warming. To enhance carbon sink efficiency, optimizing the pattern of urban blue-green coupled spaces (UBGCS) is especially important. Based on our findings, we recommend the following strategies:

(1) Strengthening the integration of hydrological networks and optimize the blue-green ratio

Regulatory thresholds should be implemented to limit the ratio of water to vegetation area through urban planning regulations. Our findings reveal a negative correlation between the blue-green area ratio (BGAR) and overall carbon sink efficiency, suggesting that an excessive water body area can limit carbon sink capacity. Therefore, the configuration of blue and green spaces should prioritize a balance between quality and efficiency, avoiding excessive occupation of vegetation space by water bodies. Additionally, reusing drainage corridors, road edges, and abandoned infrastructure as biological connectors can integrate fragmented lake wetland systems into the city's broader ecological network.

(2) Deploying multi-layer vegetation systems to enhance seasonal resilience

In high-density urban areas with limited blue-green coupled spaces, the diversity of edge habitats can be maximized by increasing the contact between blue and green spaces and designing meandering blue-green boundaries with undulating terrain. Longer water-land boundaries provide suitable habitats for vegetation, enhancing material exchange and microclimate regulation, thereby improving photosynthetic efficiency. Transforming hard revetments into natural ones and extending the contact length of blue-green spaces can enrich plant species and natural community structures, thereby enhancing carbon sink efficiency. High-carbon sink vegetation should be prioritized, and a "tree-irrigation-grass" multi-layer structure should be implemented to optimize canopy photosynthesis. A four-layer structure of trees, shrubs, herbs, and ground covers

http://www.aloki.hu ● ISSN 1589 1623 (Print) ● ISSN 1785 0037 (Online)
DOI: http://dx.doi.org/10.15666/aeer/2401_959987

will improve light energy utilization and boost summer carbon sink efficiency. Furthermore, high-carbon sink weather-tolerant species should be selected, with evergreen tree species favored for areas with low winter temperatures to maintain year-round carbon sink efficiency and avoid significant seasonal fluctuations.

(3) Implementing ecological transformation and soil improvement along lake shores

From a site design perspective, it is essential to transform hard lake shores into ecological grass slopes whenever possible. Large-scale hard paving such as roads and squares should be minimized to reduce fragmentation of the water-green space by artificial hard interfaces. This will extend the interaction interface between water and land. Additionally, targeted planting of waterside plants should be carried out. Water-tolerant species like weeping willows and Metasequoia glyptostroboides should be planted in the falling zone, while calamus and reeds can be cultivated in shallow water areas to enhance water purification. Shade-tolerant plants such as Schefflera arboricola and turtle-back bamboo can be planted in closed areas. A plant configuration of medium and small-sized trees, large flowering shrubs, and large-diameter trees, such as camphor and Metasequoia glyptostroboides, will ensure high carbon sequestration. Flowering shrubs like Lagerstroemia indica and Hibiscus syriacus can complement the tree layer, while ground cover plants such as Ophiopogon japonicus and Zephyranthes candida provide additional carbon sequestration potential. This balanced plant arrangement will not only create a rich landscape spatial hierarchy but also optimize carbon sequestration efficiency in green spaces.

Conclusions

This study establishes a quantitative relationship between the structural characteristics of urban blue-green coupled spaces (UBGCS) and carbon sink efficiency (NPP) in high-density urban areas, using multi-temporal remote sensing (2000–2020) and CASA modeling in Xiamen, China. It addresses the gap in previous research that considered only single green or blue spaces by analyzing the spatial coupling degree of UBGCS. The study reveals a fluctuating upward trend in annual NPP across Xiamen's blue-green coupled spaces, with significant seasonal variation in carbon sink efficiency. Summer NPP is more than 2.3 times higher than winter NPP, with spatial efficiency differing markedly across samples. The variability is driven by structural factors: improved carbon sequestration correlates with an increasing blue-green boundary length ratio (BGILR), where expanded interfaces enhance carbon capture through intensified water-land exchanges, and minimized fragmentation (Ci), which preserves ecological connectivity. Conversely, excessive integration degree (ID) or blue-green area ratio (BGAR) negatively impacts efficiency, as an overabundance of water coverage or non-photosynthetic vegetation hinders system functionality. Seasonally, summer efficiency is driven by BGILR, leveraging edge effects for thermal regulation and photosynthesis, while winter performance depends on the green coverage rate (GCR) to maintain root activity under cold stress. Notably, smaller sites with optimized morphology perform better than larger fragmented spaces. Based on these findings, we propose several recommendations for optimizing UBGCS layouts.

(1) Annual NPP exhibits fluctuating growth with significant seasonal variation

Quantitative assessments reveal an upward trajectory in carbon sink efficiency over the study period, with an average annual increase of 1.3% despite urban densification. Notably, summer NPP consistently exceeds winter values by a factor of 2.3, due to

http://www.aloki.hu ● ISSN 1589 1623 (Print) ● ISSN 1785 0037 (Online)
DOI: http://dx.doi.org/10.15666/aeer/2401_959987

Xiamen's subtropical climate. Summer conditions, characterized by high temperatures averaging 28℃ and elevated humidity, boost photosynthetic activity, yielding peak seasonal NPP values, such as 55.76 $gC \cdot m^{-2} \cdot a^{-1}$ in the ZSGY sample. Conversely, winter, with milder temperatures averaging 13℃ and lower moisture levels, suppresses vegetation metabolism, reducing carbon assimilation. After 2015, reduced seasonal fluctuations indicate enhanced ecological stability, likely resulting from optimized spatial configurations and vegetation management.

(2) Spatial coupling features significantly influence carbon sequestration benefits

The ratio of blue-green boundary length and fragmentation index primarily affect carbon sequestration efficiency. An extended blue-green interface length significantly enhances carbon absorption capacity, supported by a measurable positive correlation between boundary length ratio and NPP. This aligns with the edge effect theory in wetland ecology, where longer water-land interfaces enhance material exchange, microclimate regulation, and habitat diversity, thereby improving photosynthetic efficiency. Conversely, increased fragmentation index values systematically impair carbon sink functionality by disrupting ecological connectivity and hindering material circulation.

(3) Seasonal variability in carbon sink efficiency

The blue-green boundary length ratio has a much stronger positive effect in summer, while green coverage rate is more influential in winter. During summer, the boundary length ratio emerges as the primary positive regulator, utilizing edge effects to enhance thermal amelioration and photosynthetic efficiency. For example, a boundary ratio increase in cd2 from 0.6 to 0.65 led to a surge in summer NPP to 112.80 $gC \cdot m^{-2}$. In winter, carbon retention is primarily driven by green coverage density, which mitigates low-temperature stress by reducing surface heat loss and supporting root zone activity. Regions with high green coverage, such as SK, maintain stable summer NPP at 55.79 $gC \cdot m^{-2}$, demonstrating greater resilience against seasonal carbon flux volatility. These seasonal differences necessitate tailored design strategies: summer should prioritize shoreline naturalization and habitat complexity, while winter should focus on evergreen vegetation selection and microclimate buffering.

This study contributes to the systematic optimization of urban blue-green coupling spaces (UBGCS), promotes their integrated development, and provides insights for urban planning and resource management aimed at advancing the transition from low-carbon to net-zero-carbon cities. By examining carbon sequestration benefits from a spatial pattern perspective, the study offers new references for sustainable urban development.

However, several limitations should be acknowledged. The remote sensing data used had a resolution of 30 m, which affects vegetation classification, NDVI accuracy, and thus carbon sequestration estimates. Moreover, cities differ in natural geography and climate, leading to variations in the formation and spatial patterns of blue-green spaces. These factors may limit the generalizability of the findings. In addition, while this study focused on large-scale spatial patterns, finer-scale factors such as plant species, tree cover, and vegetation community structure also significantly influence carbon sequestration.

Future research should adopt a multi-scale, systematic approach and expand to include cities from diverse regions. This will help identify both common and region-specific features of UBGCS that drive carbon sequestration, thereby improving the applicability of the conclusions to broader urban contexts.

http://www.aloki.hu ● ISSN 1589 1623 (Print) ● ISSN 1785 0037 (Online)
DOI: http://dx.doi.org/10.15666/aeer/2401_959987

REFERENCES

[1] Berardi, U. (2012): Sustainability assessment in the construction sector: rating systems and rated buildings. – Sustainable Development 20(6): 411-424. https://doi.org/10.1002/sd.532.

[2] Chen, W., Feng, X., Ma, R., Hong, Q. (2016): Method of cultivated land fragmentation evaluation and empirical research: a case of Ningbo City in Zhejiang Province. – China Land Science 30: 80-87.

[3] Chen, L., Wang, Y., Zhu, E., Wu, H., Feng, D. (2024): Carbon storage estimation and strategy optimization under low carbon objectives for urban attached green spaces. – Science of The Total Environment 923: 171507. https://doi.org/10.1016/j.scitotenv.2024.171507.

[4] Cheng, L., Guan, D., Zhou, L., Zhao, Z., Zhou, J. (2019): Urban cooling island effect of main river on a landscape scale in Chongqing, China. – Sustainable Cities and Society 47: 101501. https://doi.org/10.1016/j.scs.2019.101501.

[5] Cheng, J., Huang, C., Gan, X., Peng, C., Deng, L. (2023): Can forest carbon sequestration offset industrial CO2 emissions? A case study of Hubei Province, China. – Journal of Cleaner Production 426: 139147. https://doi.org/10.1016/j.jclepro.2023.139147.

[6] Cohen, J. (1977): The significance of a product moment rs. – In: Cohen, J. (ed.) Statistical Power Analysis for the Behavioral Sciences. Academic Press, New York, NY, pp. 75-107.

[7] Dong, J., Guo, R., Lin, M., Guo, F., Zheng, X. (2024): Multi-objective optimization of green roof spatial layout in high-density urban areas—A case study of Xiamen Island, China. – Sustainable Cities and Society 115: 105827. https://doi.org/10.1016/j.scs.2024.105827.

[8] Dou, R. Y., Liang, B. Y., Li, K. Y., Zhang, C., Zhao, Y. F. (2025): The spatio-temporal coupling and coordination characteristics and spatio effects of carbon emission intensity and high-quality economic development in China. – Applied Ecology & Environmental Research 23(2): 3335-3357. http://dx.doi.org/10.15666/aeer/2302_33353357.

[9] Du, H., Cai, W., Xu, Y., Wang, Z., Wang, Y., Cai, Y. (2017): Quantifying the cool island effects of urban green spaces using remote sensing Data. – Urban Forestry & Urban Greening 27: 24-31. https://doi.org/10.1016/j.ufug.2017.06.008.

[10] Duan, W., Huang, C. (2021): Research progress on the carbon cycle of rivers and lakes. – China Environmental Science 41(8): 3792-3807.

[11] Foley, R., Kistemann, T. (2015): Blue space geographies: enabling health in place. – Health & Place 35: 157-165. https://doi.org/10.1016/j.healthplace.2015.07.003.

[12] He, Z., Lei, L., Zeng, Z. C., Sheng, M., Welp, L. R. (2020): Evidence of carbon uptake associated with vegetation greening trends in eastern China. – Remote Sensing 12(4): 718. https://doi.org/10.3390/rs12040718.

[13] Huang, D., Yi, F., Wang, S., Wei, H., Wang, S. (2022): Blue-green space pattern and indicator system in territorial planning. – City Planning Review 46: 18-31.

[14] Kaye, J. P., McCulley, R. L., Burke, I. C. (2005): Carbon fluxes, nitrogen cycling, and soil microbial communities in adjacent urban, native and agricultural ecosystems. – Global Change Biology 11(4): 575-587. https://doi.org/10.1111/j.1365-2486.2005.00921.x.

[15] Li, J., Song, C., Cao, L., Zhu, F., Meng, X., Wu, J. (2011): Impacts of landscape structure on surface urban heat islands: a case study of Shanghai, China. – Remote Sensing of Environment 115(12): 3249-3263. https://doi.org/10.1016/j.rse.2011.07.008.

[16] Marshall, M., Tu, K., Brown, J. (2018): Optimizing a remote sensing production efficiency model for macro-scale GPP and yield estimation in agroecosystems. – Remote Sensing of Environment 217: 258-271. https://doi.org/10.1016/j.rse.2018.08.001.

http://www.aloki.hu ● ISSN 1589 1623 (Print) ● ISSN 1785 0037 (Online)
DOI: http://dx.doi.org/10.15666/aeer/2401_959987

[17] Martínez-Molina, A., Tort-Ausina, I., Cho, S., Vivancos, J. L. (2016): Energy efficiency and thermal comfort in historic buildings: a review. – Renewable and Sustainable Energy Reviews 61: 70-85. https://doi.org/10.1016/j.rser.2016.03.018.

[18] Mcleod, E., Chmura, G. L., Bouillon, S., Salm, R., Björk, M., Duarte, C. M., Lovelock, C. E., Schlesinger, W. H., Silliman, B. R. (2011): A blueprint for blue carbon: toward an improved understanding of the role of vegetated coastal habitats in sequestering CO2. – Frontiers in Ecology and the Environment 9(10): 552-560. https://doi.org/10.1890/110004.

[19] Mexia, T., Vieira, J., Príncipe, A., Anjos, A., Silva, P., Lopes, N., Freitas, C., Santos-Reis, M., Correia, O., Branquinho, C., Pinho, P. (2018): Ecosystem services: urban parks under a magnifying glass. – Environmental Research 160: 469-478. https://doi.org/10.1016/j.envres.2017.10.023.

[20] Ng, E., Yuan, C., Chen, L., Ren, C., Fung, J. C. H. (2011): Improving the wind environment in high-density cities by understanding urban morphology and surface roughness: a study in Hong Kong. – Landscape and Urban Planning 101(1): 59-74. https://doi.org/10.1016/j.landurbplan.2011.01.004.

[21] Nowak, D. J., Stevens, J. C., Sisinni, S. M., Luley, C. J. (2002): Effects of urban tree management and species selection on atmospheric carbon dioxide. – Journal of Arboriculture 28(3): 113-122. https://doi.org/10.48044/jauf.2002.017.

[22] Pan, Y., Birdsey, R. A., Fang, J., Houghton, R., Kauppi, P. E., Kurz, W. A., Phillips, O. L., Shvidenko, A., Lewis, S. L., Canadell, J. G., Ciais, P., Jackson, R. B., Pacala, S. W., McGuire, A. D., Piao, S., Rautiainen, A., Sitch, S., Hayes, D. (2011): A large and persistent carbon sink in the world's forests. – Science 333: 988-993. DOI: 10.1126/science.1201609.

[23] Peng, J., Shen, H., Wu, W., Liu, Y., Wang, Y. (2016): Net primary productivity (NPP) dynamics and associated urbanization driving forces in metropolitan areas: a case study in Beijing City, China. – Landscape Ecology 31: 1077-1092. https://doi.org/10.1007/s10980-015-0319-9.

[24] Potter, C. S., Randerson, J. T., Field, C. B., Matson, P. A., Vitousek, P. M., Mooney, H. A., Klooster, S. A. (1993): Terrestrial ecosystem production: a process model based on global satellite and surface data. – Global Biogeochemical Cycles 7(4): 811-841. https://doi.org/10.1029/93GB02725.

[25] Reiman, J. H., Xu, Y. J. (2019): Dissolved carbon export and CO2 outgassing from the lower Mississippi River - Implications of future river carbon fluxes. – Journal of Hydrology 578: 124093. https://doi.org/10.1016/j.jhydrol.2019.124093.

[26] Ren, Y., Wei, X., Wang, D., Luo, Y., Song, X., Wang, Y., Yang, Y., Hua, L. (2013): Linking landscape patterns with ecological functions: a case study examining the interaction between landscape heterogeneity and carbon stock of urban forests in Xiamen, China. – Forest Ecology and Management 293: 122-131. https://doi.org/10.1016/j.foreco.2012.12.043.

[27] Short, F. T., Kosten, S., Morgan, P. A., Malone, S., Moore, G. E. (2016): Impacts of climate change on submerged and emergent wetland plants. – Aquatic Botany 135: 3-17. https://doi.org/10.1016/j.aquabot.2016.06.006.

[28] Su, M., Zheng, Y., Hao, Y., Chen, Q., Chen, S., Chen, Z., Xie, H. (2018): The influence of landscape pattern on the risk of urban water-logging and flood disaster. – Ecological Indicators 92: 133-140. https://doi.org/10.1016/j.ecolind.2017.03.008.

[29] Tan, X., Sun, X., Huang, C., Yuan, Y., Hou, D. (2021): Comparison of cooling effect between green space and water body. – Sustainable Cities and Society 67: 102711. https://doi.org/10.1016/j.scs.2021.102711.

[30] Tang, Y., Shi, T., Bu, Y., Shi, Y. (2019): Spatial distribution of soil organic carbon stocks in urban green space with urbanization in Shenyang, China. – Chinese Landscape Architecture 35: 68-73.

http://www.aloki.hu ● ISSN 1589 1623 (Print) ● ISSN 1785 0037 (Online)
DOI: http://dx.doi.org/10.15666/aeer/2401_959987

[31] Wang, F., Tang, J., Ye, S., Liu, J. (2021): Blue carbon sink function of Chinese coastal wetlands and carbon neutrality strategy. – Bulletin of Chinese Academy of Sciences 36: 241-251. https://doi.org/10.16418/j.issn.1000-3045.20210215101.
[32] Wang, J., Ke, N., Pan, J., Wang, M. (2023a): Key factors of urban blue-green spatial coupling that impact on vitality distribution characteristics: a study based on 130 samples in Changning District, Shanghai. – Landscape Architecture Academic Journal 40: 4-13, 73.
[33] Wang, J., Shen, T., Wang, M., Guo, G. (2023b): Green-blue spatial coupling design research of urban docklands in response to flooding challenge. – Landscape Architecture Academic Journal 40: 47-54.
[34] Yang, Y., Shi, Y., Sun, W., Chang, J., Zhu, J., Chen, L., Wang, X., Guo, Y., Zhang, H., Yu, L., Zhao, S., Xu, K., Zhu, J., Shen, H., Wang, Y., Peng, Y., Zhao, X., Wang, X., Hu, H., Chen, S., Huang, M., Wen, X., Wang, S., Zhu, B., Niu, S., Tang, Z., Liu, L., Fang, J. (2022): Terrestrial carbon sinks in China and around the world and their contribution to carbon neutrality. – Scientia Sinica (Vitae) 52: 534-574.
[35] Yang, S., Kong, F., Yin, H., Zhang, N., Tan, T., Middel, A., Liu, H. (2023): Carbon dioxide reduction from an intensive green roof through carbon flux observations and energy consumption simulations. – Sustainable Cities and Society 99: 104913. https://doi.org/10.1016/j.scs.2023.104913.
[36] Yang, Y., Yu, C., Li, S., Bramston, D. (2024): A planting optimization strategy to improve the carbon sink benefit for urban green-taking the communal green of Nanjing Forestry University as an example. – Ecological Indicators 159: 111619. https://doi.org/10.1016/j.ecolind.2024.111619.
[37] Yu, Z., Yang, G., Zuo, S., Jørgensen, G., Koga, M., Vejre, H. (2020): Critical review on the cooling effect of urban blue-green space: a threshold-size perspective. – Urban Forestry & Urban Greening 49: 126630. https://doi.org/10.1016/j.ufug.2020.126630.
[38] Yu, J., Zhou, Y., Wang, X., Guo, S. (2021): Influence of urban blue-green landscape pattern on rainfall-flood regulation and storage function. – Landscape Architecture 28: 63-67.
[39] Yuan, Y., Tang, S., Zhang, J., Guo, W. (2023): Quantifying the relationship between urban blue-green landscape spatial pattern and carbon sequestration: a case study of Nanjing's central city. – Ecological Indicators 154: 110483.
[40] Yuan, Y., Guo, W., Tang, S., Zhang, J. (2024): Effects of patterns of urban green-blue landscape on carbon sequestration using XGBoost-SHAP model. – J. Clean. Prod. 476: 143640. https://doi.org/10.1016/j.jclepro.2024.143640.
[41] Zhang, Y., Meng, W., Yun, H., Xu, W., Hu, B., He, M., Mo, X., Zhang, L. (2022): Is urban green space a carbon sink or source? - A case study of China based on LCA method. – Environmental Impact Assessment Review 94: 106766. https://doi.org/10.1016/j.eiar.2022.106766.
[42] Zhang, J., Yuan, J., Zuo, J., Mao, R. (2025): Unveiling the spatiotemporal dynamics and sectoral nexus of urban carbon metabolism: insights from community-level analysis. – Journal of Environmental Management 393: 127036. https://doi.org/10.1016/j.jenvman.2025.127036.
[43] Zhao, H., Hu, M., Zhu, J., Huang, T., Zhang, Y., Li, Y., Yan, M. (2023): Blue-green space cooling effect and its influencing factors in metropolitan area: a case study on the area within the Fifth Ring Road in Beijing. – Acta Ecologica Sinica 43: 4904-4919.
[44] Zhou, C., Mao, Q., Xu, X., Fang, C., Luo, Y., Li, B. (2016): Preliminary analysis of c sequestration potential of blue carbon ecosystems on Chinese coastal zone. – Scientia Sinica (Vitae) 46: 475-486.
[45] Zhou, P., Hou, H., Zhang, H., Liu, X., Tan, W. (2021): The development prospects and implementation suggestions of increasing soil carbon storage in the context of carbon neutrality. – Environmental Protection 49: 63-67.

http://www.aloki.hu ● ISSN 1589 1623 (Print) ● ISSN 1785 0037 (Online)
DOI: http://dx.doi.org/10.15666/aeer/2401_959987

[46] Zhu, W., Pan, Y., Zhang, J. (2007): Estimation of net primary productivity of Chinese terrestrial vegetation based on remote sensing. – Chinese Journal of Plant Ecology 31(3): 413-424. DOI: 10.17521/cjpe.2007.0050.

http://www.aloki.hu ● ISSN 1589 1623 (Print) ● ISSN 1785 0037 (Online)
DOI: http://dx.doi.org/10.15666/aeer/2401_959987

APPENDIX

Table S1. *Summary of key basic landscape indicators of blue–green coupled space on Xiamen Island (2000–2020)*

Site	Year	TBGSA (m^2)	GSA (m^2)	WSA (m^2)	GCR (%)
ZSGY	2000	70200	67500	2700	58.5938
ZSGY	2005	76500	73800	2700	63.5659
ZSGY	2010	70200	67500	2700	58.5938
ZSGY	2015	76500	73800	1800	64.3411
ZSGY	2020	70200	68400	1800	59.375
cd2	2000	80100	71100	9000	60.3053
cd2	2005	86400	78300	8100	67.4419
cd2	2010	78300	70200	8100	59.542
cd2	2015	85500	77400	8100	66.6667
cd2	2020	72900	68400	4500	58.0153
cd3	2000	18900	11700	7200	18.8406
cd3	2005	15300	7200	8100	12.5
cd3	2010	14400	4500	9900	7.2464
cd3	2015	16200	7200	9000	12.5
cd3	2020	14400	7200	7200	11.5942
cd4	2000	127800	17100	110700	10.7345
cd4	2005	126900	16200	110700	10.2273
cd4	2010	121500	18900	102600	11.8644
cd4	2015	108900	12600	96300	7.9545
cd4	2020	108000	14400	93600	9.0395
SDGY	2000	855900	430200	425700	44.7985
SDGY	2005	854100	540900	313200	54.3891
SDGY	2010	765000	550800	214200	57.3571
SDGY	2015	793800	626400	167400	62.9864
SDGY	2020	742500	562500	180000	58.5754
SK	2000	1053000	236700	816300	19.8791
SK	2005	1021500	209700	811800	17.4010
SK	2010	945000	189000	756000	15.873
SK	2015	979200	216000	763200	17.9238
SK	2020	950400	177300	773100	14.8904
cd6	2000	54900	47700	7200	22.6496
cd6	2005	62100.0000	40500	21600.0000	20.6422
cd6	2010	54900	29700	24300	14.1026
cd6	2015	63900.0000	36900	27000.0000	18.8073
cd6	2020	54900	36000	18000	17.094
cd7	2000	1450800	320400	1130400	13.6086
cd7	2005	1476000.0000	319500.0000	1156500.0000	13.6696
cd7	2010	1475100	280800.0000	1194300	11.9266
cd7	2015	1477800.0000	292500	1185300.0000	12.5144
cd7	2020	1475100	299700	1175400	12.7294
cd8	2000	41400	11700.0000	29700	8.2803
cd8	2005	18900.0000	13500.0000	5400.0000	8.9820
cd8	2010	21600	11700.0000	9900	8.2803
cd8	2015	18900.0000	12600.0000	6300.0000	8.3832
cd8	2020	21600	15300.0000	10800	10.828

Note: GSA: Green Space Area; WSA: Water Surface Area; GCR: Green Coverage Rate; TBGSA: Total Blue-Green Space Area; BGAR: Blue-Green Area Ratio; ID: Integration Degree; Ci: Fragmentation Index. ZSGY: Zhongshan Park; cd2: Huli Park; cd3: Torch Park; cd4: Dialiao Reservoir Park; SK: Hubian Reservoir Park; SDGY: Wuyuan Bay Wetland Park; cd6:Yuandang Neihu area; cd7: Yuandang Hu area; cd8: Bay Park

http://www.aloki.hu ● ISSN 1589 1623 (Print) ● ISSN 1785 0037 (Online)
DOI: http://dx.doi.org/10.15666/aeer/2401_959987

Table S2. *Summary of key coupling relationship indicators of Blue–Green Coupled Space on Xiamen Island (2000–2020)*

Site	Year	BGIL	BGILR	SLW	BGAR	ID	Ci
ZSGY	2000	210	0.7000	1.1401	0.0400	0.9615	26.0417
ZSGY	2005	270	0.75	1.465807536	0.036585366	0.964705882	31.0078
ZSGY	2010	210	0.7	1.4101	0.04	0.9615	26.0417
ZSGY	2015	180	0.75	1.196826841	0.024096386	0.964705882	15.9681
ZSGY	2020	120	0.6667	0.7979	0.0263	0.9744	15.625
cd2	2000	360	0.6	1.0705	0.1266	0.8876	50.8906
cd2	2005	390	0.65	1.222410764	0.103448276	0.90625	51.6796
cd2	2010	360	0.6	1.1284	0.1154	0.8966	50.8906
cd2	2015	390	0.65	1.222410764	0.104651163	0.905263158	51.6796
cd2	2020	90	0.3	0.3785	0.0658	0.9383	25.4453
cd3	2000	30	0.1	0.0997	0.6154	0.619	48.3092
cd3	2005	150	0.625	0.470157986	1.125	0.470588235	41.6667
cd3	2010	30	0.1	0.0851	2.2	0.3125	48.3092
cd3	2015	150	0.5	0.446031029	1.25	0.444444444	52.0833
cd3	2020	150	0.625	0.4987	1	0.5	38.6473
cd4	2000	540	0.439	0.4578	6.4737	0.1338	77.2128
cd4	2005	510	0.5	0.432405723	6.833333333	0.127659574	510
cd4	2010	360	0.3429	0.317	5.4286	0.1556	360
cd4	2015	300	0.27027027	0.272711329	7.642857143	0.115702479	300
cd4	2020	360	0.3243	0.3319	6.5	0.1333	69.6798
SDGY	2000	5730	0.8197	2.4774	0.9895	0.5026	74.31
SDGY	2005	6630	0.856589147	3.341932853	0.579034942	0.633298209	77.8281
SDGY	2010	5130	0.7246	3.1268	0.3889	0.72	73.727
SDGY	2015	4860	0.84375	3.350839377	0.267241379	0.789115646	57.9186
SDGY	2020	4710	0.801	3.1317	0.32	0.7576	61.2309
SK	2000	5250	0.7813	1.6392	3.4487	0.2248	72.7898
SK	2005	4650	0.6858	1.455873019	3.871244635	0.205286344	56.2609
SK	2010	4290	0.5837	1.3918	4	0.2	61.7284
SK	2015	5010	0.6680	1.617758212	3.533333333	0.220588235	62.2355
SK	2020	4500	0.6522	1.4437	4.3604	0.1866	57.9491
cd6	2000	420	0.5385	1.3963	0.1509	0.8689	37.037
cd6	2005	540	0.620689655	1.036482448	0.533333333	0.652173913	44.3425
cd6	2010	570	0.4318	1.0315	0.8182	0.55	62.6781
cd6	2015	520	0.444444444	0.8927226	0.731707317	0.577464789	128.4404
cd6	2020	600	0.5882	1.2616	0.5	0.6667	48.433
cd7	2000	5400	0.3557	1.4328	3.5281	0.2834	64.475
cd7	2005	5070	0.344897959	1.329934367	3.61971831	0.216463415	62.8931
cd7	2010	5100	0.3288	1.3165	4.2532	0.2351	65.8767
cd7	2015	5280	0.355555556	1.368090567	4.052307692	0.197929354	63.5348
cd7	2020	5670	0.375	1.4753	3.9219	0.255	64.2202
cd8	2000	30	0.0286	0.0491	2.5385	0.2826	74.31
cd8	2005	0	0	0	0.4	0.7143	15.9681
cd8	2010	0	0	0	1.1818	0.7083	23.3546
cd8	2015	0	0	0	0.5	0.666666667	17.9641
cd8	2020	0	0.0000	0	0.7059	0.5862	25.4777

Note: GIL: Blue–Green Interface Length; BGILR: Blue–Green Interface Length Ratio; SLW: Shape Index of Blue–Green Boundary; BGAR: Blue–Green Area Ratio; ID: Integration Degree; Ci: Fragmentation Index. ZSGY: Zhongshan Park; cd2: Huli Park; cd3:Torch Park; cd4: Dialiao Reservoir Park; SK: Hubian Reservoir Park; SDGY: Wuyuan Bay Wetland Park; cd6:Yuandang Neihu area; cd7: Yuandang Hu area; cd8: Bay Park

http://www.aloki.hu ● ISSN 1589 1623 (Print) ● ISSN 1785 0037 (Online)
DOI: http://dx.doi.org/10.15666/aeer/2401_959987